Andrea Zünterl BSc BSc

New insights to the formation of modern dolomite in a continental low temperature environment – A case study from the Erzberg (Styria, Austria)

MASTER'S THESIS

to achieve the university degree of

Master of Science

Master's degree programme: Geoscience

submitted to

Graz University of Technology

Supervisor

Dr. rer. nat. M. Sc. Andre Baldermann

Univ.-Prof. Dipl.-Min. Dr. rer. nat. Martin Dietzel

Institute of Applied Geosciences

Graz, October 2019

AFFIDAVIT

I declare that I have authored this thesis independently, that I have not used other than the declared sources/resources, and that I have explicitly indicated all material which has been quoted either literally or by content from the sources used. The text document uploaded to TUGRAZonline is identical to the present master's thesis dissertation.

_____ _____

Date Signature

ACKNOWLEDGMENTS

Judith Jernej, Sylvia Perchthold, Andrea Wolf and Maria Hierz are thanked for their assistance in the laboratory at the Graz University of Technology, Institute of Applied Geosciences (IAG). Stable carbon and oxygen isotope values were measured by Albrecht Leis at the JR-AquaConSol GmbH. Helmut Mühlhans prepared the thick sections at the Montanuniversity of Leoben. I thank Florian Mittermayr (Institute of Technology and Testing of Construction Materials) and Cyrill Grengg (IAG) for assistance with EMPA analysis, including imaging and acquisition of element distribution mappings and quantitative point measurements. Dorothee Hippler is greatly acknowledged for Mg isotope measurements at the NAWI Graz Central Laboratory for Water, Minerals and Rocks at IAG. I particularly wish to thank the VA Erzberg GmbH for the possibility to take samples at the open pit mine. In this connection, I also want to acknowledge Ronny Boch (IAG) for his help during the field work, for the provision of modern water samples from the Erzberg and his adjuvant comments on this study. Many thanks are depicted to Martin Dietzel, Head of working group Mineralogy and Hydrogeochemistry at IAG, for his helpful suggestions and improvements on this thesis. Especially I would like to express my gratitude to Andre Baldermann (IAG) for all the time he spent on performing ICP-OES analyses, for explaining XRD quantification methods and for the very helpful discussions as well as a lot of constructive response.

ABSTRACT

The mineral dolomite [$CaMg(CO_3)_2$] is highly abundant in ancient marine sedimentary based successions. However, modern dolomite forming environments are scarce and often restricted to marine evaporitic and reductive sediments, where microbial activity and related metabolic products facilitate dolomitization. Rare occurrences of Quaternary dolomite deposits have been also reported from alkaline lakes as well as from karst and cave settings, although the timing, process and physicochemical conditions for dolomitization in such continental surroundings remain questionable until recent. In order to elucidate the driving factors for dolomitization in a continental, low temperature environment, carbonate vein deposits (aragonite and two types of sedimentary dolomite) from the Erzberg (Styria, Austria) have been discovered and investigated for their petrography, mineralogy and geochemistry. The obtained results reveal two generations of authigenic dolomite at the Erzberg, which are sandwiched by whitish laminae of aragonite and minor calcite deposits in an alternate mode, known as erzbergite. U-Th age determinations of aragonite indicate “old” dolomite spheroids precipitated at around the last Glacial Maximum (~19-18 kyr BP), whereas “young” matrix dolomite formed from approx. 14 kyr BP onward. Based on the combination of X-ray diffraction and electron microprobe analyses the spheroidal “old” dolomite is considered to be near-stoichiometric (~51 mol% $CaCO_3$) with a moderate degree of cation ordering (0.35) and displaying zonation pattern (Ca-rich cores; Mg-rich rims). Matrix-replaced “young” dolomite is characterized by Ca-excess (~54 mol% $CaCO_3$), a low degree of cation ordering (0.25) without zonation pattern. Replacement textures and clumped isotopic signatures (Δ_{47}) of the authigenic Ca-Mg carbonates as well as compositions of modern water draining the Erzberg suggest the matrix dolomite precipitated (i) on the extent of aragonite or/and low-Mg calcite at high aqueous Mg:Ca ratios of the mineralizing (meteoric) fluids and (ii) at very low to ambient temperatures (ca. 3 to 20 °C). Analysis of the $\delta^{18}O$, $\delta^{13}C$ and $^{87}Sr/^{86}Sr$ isotopic values of the fracture carbonates, host rocks and locally draining water at the Erzberg indicate that infiltration of meteoric solutions along vertical fractures induced host rock dissolution (Sauberger Kalk and iron ore carbonates). Initial erzbergite (aragonite) precipitation caused Mg vs. Ca enrichment in the remaining solution with molar Mg:Ca ratios between 13 and 26. Subsequently the elevated Mg:Ca ratios induced dolomite precipitation and/or dolomitization of the former precursor phases (e.g. aragonite, low-Mg calcite). This exotic outstanding Ca-Mg carbonate vein mineralization at near-freezing conditions represents a novelty in dolomite research on continental-meteoric settings. Accordingly, such fracture dolomites should be considered in future studies on paleo-environmental reconstruction, in analogy to modern marine equivalents.

KURZFASSUNG

Das Mineral Dolomit [$CaMg(CO_3)_2$] ist häufig in alten marinen sedimentären Abfolgen anzutreffen. Jedoch sind die Bildungsbereiche von rezentem Dolomit rar und meist beschränkt auf marine-evaporitische Sedimente und reduzierende Bedingungen, bei denen mikrobielle Aktivität und damit verbundene Stoffwechselprodukte eine Dolomitisierung favorisieren. Seltene Vorkommen von quartärem Dolomit wurden bisher für alkalische Seen sowie für Karst und Höhlen Umfelder beschrieben. Der Zeitablauf, der Reaktionsablauf und die physikochemischen Bedingungen, welche die Dolomitisierung in derartigen kontinentalen Umgebungen ermöglichen, blieben bisher ungeklärt. Um die steuernden Faktoren für die Dolomitisierung in kontinentalen, niedrig Temperatur Umgebungen zu untersuchen, wurden Karbonat-Gang-Ablagerungen (Aragonit und zwei Typen sedimentärer Dolomit) vom Erzberg (Steiermark, Österreich) erkannt und auf deren Petrographie, Mineralogie und Geochemie hin analysiert. Die erhaltenen Resultate zeigen zwei Generationen von authigenem Dolomit am Erzberg, welche durch weißliche Laminä, bestehend aus Aragonit und untergeordnet Kalzit, abgegrenzt werden. Diese Wechsellagerung von Aragonit und Kalzit wird als Erzbergit bezeichnet. Das U-Th Alter des Aragonits deutet darauf hin, dass der „alte“ sphäroidale Dolomit rund um das letzteiszeitliche Maximum (~ 19-18 kyr BP) gebildet wurde, wohingegen der „junge“ Matrix-Dolomit vor weniger als 14 kyr BP gebildet wurde. Die Kombination von Röntgendiffraktometrie- und Elektronstrahlmikro-Analysen zeigen einen nahezu stöchiometrischen „alten“ Dolomit (~51 mol% $CaCO_3$) mit einen mäßigen Grad an Kationenordnung (0.35) und ausgeprägter Zonierungen innerhalb der Kristalle (Ca-reiche Kerne und Mg-reiche Ränder). Der Matrix ersetzende Dolomit ist durch einen Ca-Überschuss (~54 mol% $CaCO_3$) sowie niedrigerem Kationenordnungsgrad (0.25) charakterisiert und zeigt keine Zonierungsmuster. Ersatz- und Austauschtexturen sowie Clumped Isotope ($\Delta 47$) Signaturen der authigenen Ca-Mg Karbonate als auch die Zusammensetzung der rezenten Wässer, welche den Erzberg entwässern, weisen darauf hin, dass Matrix-Dolomit (i) auf Kosten von Aragonit oder/und niedrig-Mg Kalzit bei hohen wässrigen Mg:Ca Verhältnissen des mineralisierenden (meteorischen) Fluids und (ii) bei sehr niedrigen Temperaturen bis Umgebungstemperatur (ca. 3 bis 20 °C) gebildet wurde. Des Weiteren wurde die isotopische Zusammensetzung der Störungs-Karbonate, der unterschiedlichen Muttergesteine sowie des meteorischen Wassers am Erzberg mittels Analysen wie $\delta^{18}O$, $\delta^{13}C$ und $^{87}Sr/^{86}Sr$ untersucht. Die Ergebnisse belegen, dass es durch die Infiltration von meteorischen Lösungen entlang von vertikalen Klüften und Störungen zu einer Lösung des Muttergesteins (Sauberger Kalk und Eisenerz) kommt. Anschließend wird Erzbergit (Aragonit) initial präzipitiert, wodurch die Mg vs. Ca Konzentration in der Lösung ansteigt und schließlich zu einem Mg:Ca Verhältnis von 13 bis 26 führt, was wiederum dazu führt, dass Dolomit gebildet wird bzw. eine vorhanden

Vorgängerphase (z.B. Aragonit, niedrig-Mg Kalzit) dolomitisiert wird. Diese exotischen, außerordentlichen Ca-Mg Karbonate, die sich in Klüften bei Bedingungen nahe dem Gefrierpunkt gebildet haben, repräsentieren eine Neuheit in der Dolomit-Forschung in kontinental-meteorischen Settings. Solche Störungs-Dolomite sollten in zukünftigen Paläo-Umwelt-Rekonstruktionsstudien berücksichtig werden, ähnlich wie bei den modernen marinen Äquivalenten.

TABLE OF CONTENTS

1. INTRODUCTION

Sedimentary based dolomite [$CaMg(CO_3)_2$] is a volumetrically important rock-forming mineral in ancient carbonate rocks, but its occurrence in modern-marine carbonate-depositing environments is scarce in spite of the fact that modern seawater is highly supersaturated with respect to dolomite (Lippmann, 1973; Warren, 2000; Baldermann et al., 2015). Special conditions, like high temperatures (> 150 °C) and high aqueous Mg:Ca molar ratios (> 10:1) enable dolomite formation in laboratory experiments, whereas inorganic dolomite precipitation at ambient temperature failed, despite e.g. 1000-fold supersaturation and reaction times up to 32 years (Land, 1998). This enigma is referred to the ”dolomite problem” (Irion and Müller, 1968; Müller, 1970; Müller et al., 1972; Middelburg et al., 1990; Land, 1998; Alonso-Zarza and Martín-Pérez, 2008; Dupraz et al., 2009; Sánchez-Román et al., 2009; Warren, 2000; Geske et al., 2015; Baldermann et al., 2015; Veetil et al., 2018). Several models have been developed to explain the massive occurrences of sedimentary based dolomite in ancient platform carbonates, ranging from direct dolomite precipitation from supersaturated solutions to replacement of calcium carbonate (limestone) precursors through interaction with Mg-rich fluids during burial diagenesis (Warren, 2000; Baldermann et al., 2015). Many studies have suggested that microbial activity is a key factor relating to dolomite formation at low temperature, because associated processes, like bacterial sulphate reduction and secretion of exopolymeric substances (EPS), lead to a reduction of the kinetic energy barriers that prevent the precipitation of dolomite from supersaturated solutions (Vasconcelos et al., 1995; Vasconcelos and McKenzie, 1997; Land, 1998; Warthmann et al., 2005; Bontognali et al., 2010; Deng et al., 2010; Baldermann et al., 2015). Accordingly, sulphate-reducing bacteria and EPS can create a micro environment suitable for authigenic dolomite formation (Warthmann et al., 2005; Bontognali et al., 2010). Bontognali et al. (2014) stated that EPS is responsible for the formation of Ca-excess dolomite and very high-Mg calcite (VHMC) under Earth`s surface conditions, because it helps triggering Mg^{2+} ion dehydration, hence providing higher concentration of Mg^{2+} ions for the dolomitization process. The precipitated near-stoichiometric Ca-Mg carbonates very often do not show a high degree of structural order (e.g. in ideal dolomite, Ca and Mg are distributed in alternating cation layers within the carbonate lattice), hence they are commonly referred to as proto-dolomite (Baldermann et al., 2015).

From the study of modern and past dolomite forming settings it can be inferred that high aqueous Mg:Ca molar ratios, microbial activity, presence of seeds, elevated Fe^{2+} concentrations, high dissolved sulphide concentrations, low sulphate concentrations, high carbonate alkalinity, alkaline pH and high temperatures favour the nucleation and the subsequent crystal growth of dolomite during early marine diagenesis (Lippmann, 1973; Land, 1980; Vasconcelos et al., 1995; Warren, 2000; Geske et al., 2015; Baldermann et al., 2015).

Baldermann et al. (2015) have mentioned that the preferable requirements for recent dolomite formation comprise evaporitic and marine-anoxic settings, in combination with sulphate reduction in organic-rich sediments. Such conditions occur, for example, in the sabkha environments of Abu Dhabi and in the Coorong Region (South Australia) (e.g. (Wacey et al., 2007; Bontognali et al., 2010), as well as in the hypersaline coastal lagoons at Lagoa Vermelha (Brazil) (e.g. (Vasconcelos and McKenzie, 1997; Warthmann et al., 2005). At Deep Springs Lake (California, USA), which represents a highly alkaline playa lake, recent dolomite formation was also observed. It has been proposed that the direct precipitation of dolomite from highly alkaline brines is driven by high carbonate alkalinity (Meister et al., 2011). On the other hand, (proto-)dolomite precipitations have also been observed in non-marine (e.g. lacustrine) environments, like at Lake Neusiedel (Austria) and Lake Balaton (Hungary) (Müller, 1970; Müller et al., 1972), so that the physicochemical conditions linked to dolomite formation at low temperature still remain a matter of intense scientific debate.

Very recently, De Boever et al. (2017) have revisited the various non-marine environments, where dolomitization can take place, and have subdivided them into to the following groups: (1) karst and cave deposits (Castanar cave, Spain), (2) pedogenic precipitates (calcretes and dolocretes in the Madrid Basin, Spain), (3) hot and cool spring and stream deposits (Lazio, Central Italy) and (4) marginal, lacustrine-palustrine sediments (Lac Leman, Switzerland and Great Salt Lake, USA). The origin of fluids responsible for dolomitization in these settings is highly complex, ranging from freshwater and marine or mixed marine-meteoric fluids to subsurface or burial diagenetic fluids (Flügel, 2004; Moore and Wade, 2013; Swart, 2015; De Boever et al., 2017). Though the precise processes underlying dolomite formation in non-marine environments are not fully understood yet, it has been widely accepted that Ca-Mg carbonate and dolomite formation follows the primary dolomitization model (direct precipitation from the solution followed by dissolution and reprecipitation processes. For more details see Warren (2000)), whereas only a minor percentage of dolomite could have been emerged from biogenic secretion (De Boever et al., 2017). However, compared to the marine realm the occurrence of Ca-Mg carbonates, and dolomite in particular, in continental, low temperature environments is scarce (Alonso-Zarza and Martín-Pérez, 2008). Only a few studies have reported on the formation of carbonates in the cryogenic environment, i.e. basically calcite precipitation under permafrost conditions has been described (Žák et al., 2004; Richter et al., 2010; Žák et al., 2018).

Recently, Boch et al. (2019) have investigated young authigenic Ca-carbonate formations in (active) fault zones at the Erzberg (Styria, Austria) - known as erzbergite (e.g., alternating laminated sequences of aragonite and minor calcite). These vein precipitates have been deposited between 285.1 ± 3.9 to 1.03 ± 0.04 kyr BP at precipitation temperatures between 0 to 10°C, indicating formation at near-freezing temperatures in geologically young to recent

times. During later works, carbonate cataclasites containing Ca-excess dolomite and aragonite in close vicinity have been discovered, also suggesting a low temperature origin of the fracture dolomite. However, the nature of the Erzberg dolomite has not been investigated further so far. Therefore, the present study focuses on the mineralogical, microstructural, isotopic and geochemical characterization of the vein dolomites from the Erzberg. The environmental key parameters and fundamental processes leading to the formation of aragonite and in particular dolomite in this exotic (continental and low temperature) surrounding are discussed in a broader context.

2. GEOLOGICAL SETTING

The Erzberg is located 50 km NW of Graz (Styria, Austria) and is part of the Noric nappe system within the Greywacke zone in the Northern Calcareous Alps (Fig. 1A). This famous study site (so-called the 'Erzberg iron ore deposit') represents the largest siderite ($FeCO_3$) deposit worldwide and is considered to be one of the most prominent geological places in Austria due to its outstanding historic, economic and scientific value (Boch et al., 2019). The various siderite mineralizations and head beds of intergrown siderite and ankerite ($Ca(Fe,Mg,Mn)(CO_3)_2$; also known as 'Rohwand') at the Erzberg are actively mined by the VOEST-ALPINE Erzberg Ges.m.b.H. The present-day`s Austrian iron ore production is entirely generated from this mine and amounts to about 2 million tons per year (Prochaska, 2012; Prochaska, 2016).

The architecture of the Erzberg is characterized by a tectonic duplication of the Paleozoic carbonate rocks (Fig. 2). The Late Ordovician, represented by the Blasseneck porphyroid, is overlain by Silurian and Devonian marine limestone sequences, about 230 m thick (Fig. 1B). After an erosional gap in the Viséan (Carboniferous), thin layers of limestone breccia and quartzitic shales ('Eisenerz-Formation') were deposited. The Middle to Upper Permian 'Präbichl Formation' (also known as Red Beds, e.g. consisting of sandstones, shales and conglomerates) and the Lower Triassic 'Werfen Formation' (e.g. limestone and shale breccia) superpose the duplicated Silurian and Devonian sequences, which also includes the main iron ore body. In the last decades, two different genetic models have been developed in attempt to explain the origin of the Erzberg iron ore deposit: (A) metasomatic epigenetic origin in which reducing, Fe-rich hydrothermal fluids have infiltrated the Devonian limestones and the Permian carbonate conglomerates, leading to siderite mineralizations by replacement (e.g. (Spindler, 1992; Prochaska, 1997; Prochaska, 2012; Belocky, 1992; Prochaska, 2016; Meixner, 1970; Schulz et al., 1997), and (B) primary syngenetic origin, where the iron ore has been formed by synsedimentary, volcanogenic processes (Schouppe, 1854; Vacek, 1900; Beran and Thalmann, 1977). Petrographic analyses of the siderite layers support the first model; however, the precise mechanisms underlying the formation of the main iron ore body are not completely understood, yet.

The Erzberg section underwent two main stages of tectonic activity, e.g. metamorphic overprinting during the Variscan orogeny to within the lower greenschist facies and tectonic duplication of the mostly Devonian rocks due to the development of the Alpine Thrust Fold in the Cretaceous. During the Alpine tectonic synclinal deformation and later gravitational mass movement many (young) faults have been emerged and are now passing in a NNE-direction through the Erzberg. Subsequent strain-tectonics caused further the development of a normal

faulting system (dip: 20-30° E), including the so-called “Christoph-Hauptverwurf”, a steep SE oriented main fault, and the “Vordernberger Hauptverwurf” fault with a steep NNE dip (Schönlaub, 1982; Prochaska, 2012; Boch et al., 2019). In some of these fractures carbonate sinter of variable mineralogy (calcite and aragonite) and thickness (centimeters to several decimeters) have been recognized earlier in the mining history of the Erzberg (Hatle, 1892; Angel, 1939).

Radiometric U-Th age dating of the prominent $CaCO_3$ vein precipitates (i.e. intercalated laminae of aragonite and calcite; the so-called erzbergite) have shown that the majority of the erzbergite is very young: The older ones ranging from 285.1 ± 3.9 kyr BP to 55.54 ± 0.27 kyr BP and the younger ones from 10.41 ± 0.17 kyr BP to 1.03 ± 0.04 kyr BP, respectively (Boch et al., 2019). Hence, the younger carbonate formations have been deposited up to very recent times. A very precise age control was recently established for the erzbergite deposits occurring at the southern section of the Erzberg, where the dolomitized sections also crop out: precipitation ages of about 19.21 ± 0.10 kyr BP to 13.11 ± 0.09 kyr BP have been observed (unpublished data: R. Boch).

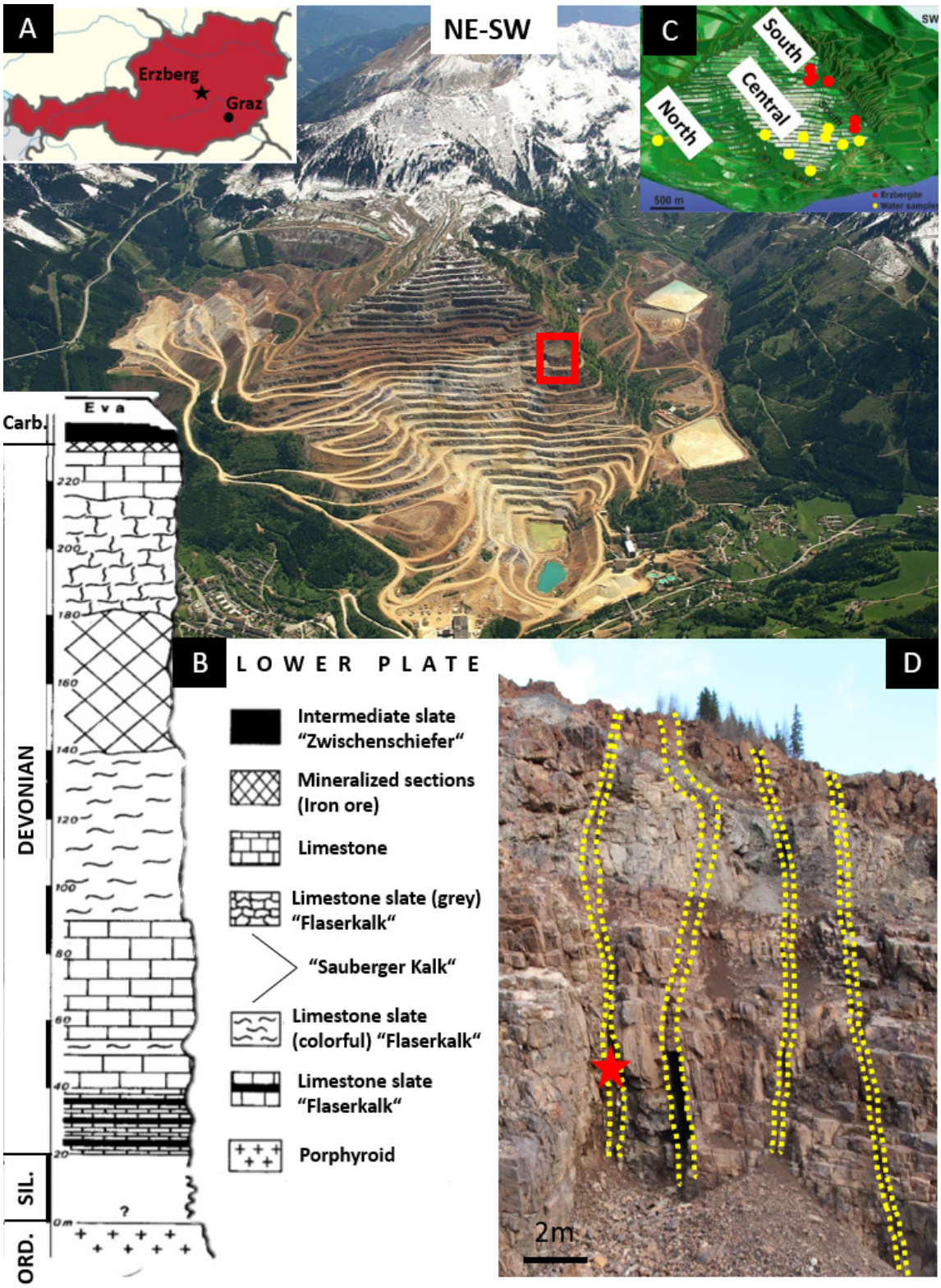

***Fig. 1**: (A) Location map of the Erzberg iron ore deposit (Styria, Austria) with the sampling location in the southwestern section at the so-called "Schuchart Etage" (labeled with red rectangle) (photograph origin by Bavaria Luftbild Verlags GmbH). (B) Lithostratigraphic profile (near sample location) of the Erzberg succession established based on conodonts and other macrofossils modified from Schönlaub et al. (1980). (C) Digital surface model of the Erzberg showing the positions of sampled carbonate precipitates in fractures (erzbergite in red) and aqueous solutions (fracture and surface waters in yellow) (modified from Boch et al., 2019). (D) Closer look of the sampling location (marked in A) showing parallel faults that are partly filled with intercalated aragonite and calcite laminae (erzbergite) and carbonate cataclasites. The red star denotes the position of the obtained samples.*

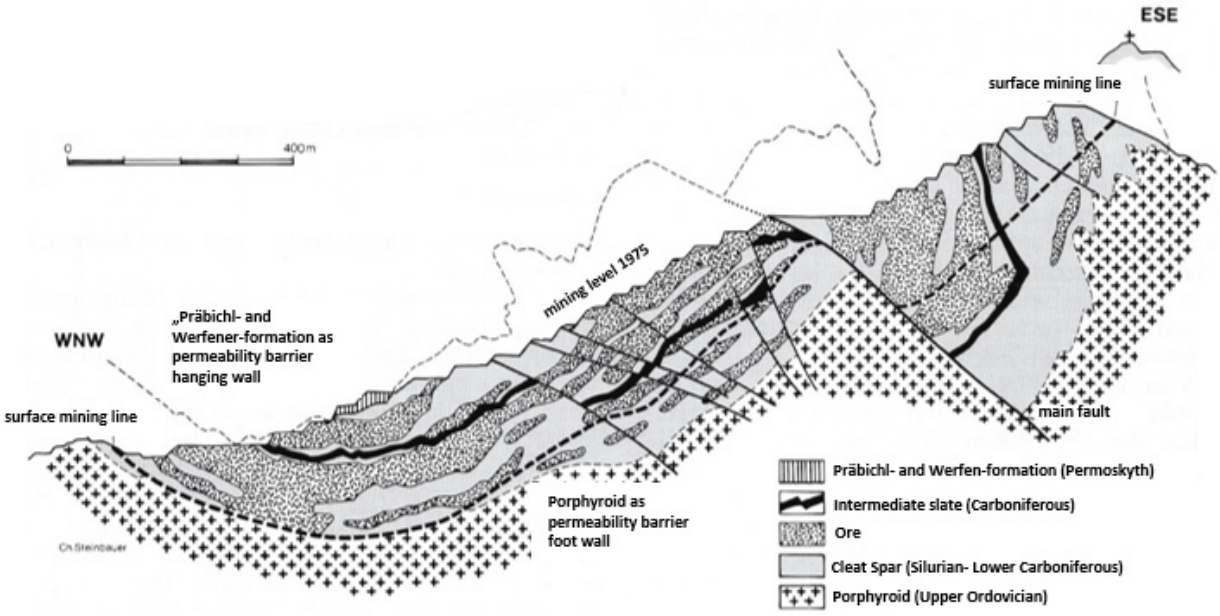

***Fig. 2**: Geological cross section through the Styrian Erzberg displaying the position of main siderite ore deposits as well as the tectonic duplication of the Paleozoic carbonate host rocks (modified from Prochaska, 2012).*

2.1. Modern hydrogeochemistry and carbonate formation temperatures

Based on the collection and subsequent hydrochemical characterization of modern drip waters, gathered from several locations at the northern, central and southern sections of the Erzberg (Fig. 1C), three different water types have been identified by Boch et al. (2019): Mg-HCO_3, Mg-Ca-HCO_3 and Mg-Ca-HCO_3-SO_4. Important hydrochemical parameters and isotopic compositions of these waters are summarized in Table 1. However, from these waters, only those from the southern parts are particularly relevant for this study, as they actively drain the area containing the dolomitized carbonate cataclasites under investigation. In detail, the southern (Mg-HCO_3-type) water is characterized by pH 8.74 ± 0.04, electric conductivity (EC) of 877 ± 86 µS/cm and a water temperature of 21.2 ± 5.0°C. The chemical composition of this water is dominated by 128 ± 15 mg/l of Mg^{2+}; 12 ± 2 mg/l of Ca^{2+}; 604 ± 59 mg/l of HCO_3^- and 59 ± 16 mg/l of SO_4^{2-}. Accordingly, this drip water is highly supersaturated with respect to the $CaCO_3$ polymorphs, aragonite and calcite (Table 1). The calculated carbon dioxide (CO_2) partial pressures exhibit slightly increased values (log P_{CO2} of -3.2 to -3.0), compared to ambient atmospheric values (log P_{CO2} of ca. -3.3). Moreover, stable isotope analyses yield δ^2H values from -68.1 to -55.2‰ (VSMOW), while $\delta^{18}O$ values range from -9.1 to -7.7‰ (VSMOW) (Boch et al., 2019). In addition, $\delta^{13}C_{DIC}$ varies in the range from +3.5 to +3.7‰ (VPDB), and $\delta^{34}S$ values of dissolved sulphate in solution range from -4.9 to +2.5‰ (VCDT); $\delta^{34}S$ have only been measured in the central section (see Boch et al., 2019). Supplementary, radiogenic Sr isotope compositions (expressed as $^{87}Sr/^{86}Sr$) of drip waters from all sections at the Erzberg have been investigated to trace carbonate provenance (unpublished data: A. Baldermann).

In the present study, waters from the southern section have been investigated further regarding Mg isotopes and modelling of aqueous speciation and saturation indices of relevant Ca-Mg carbonates in order to gain a better understanding of modern erzbergite- and dolomite-forming processes.

***Table 1**: Compilation of hydrochemical parameters of drip waters taken from the northern, central and southern sections of the Erzberg (from Boch et al., 2019). Note that one water sample from the southern section was not taken into consideration.*

Parameter	North (n=1)	Central (n=4)	South (n=4)
Temperature [°C]	14.1	12.6 ± 2.7	21.2 ± 5.0
EC [µsec/cm]	488	1383 ± 58	877 ± 86
pH	8.40	8.15 ± 0.05	8.74 ± 0.04
Ca^{2+} [mg/l]	43	97 ± 7	12 ± 2
Mg^{2+} [mg/l]	42	139 ± 12	128 ± 15
Cl^{-} [mg/l]	1	27 ± 6	5 ± 3
HCO_3^{-} [mg/l]	326	700 ± 61	604 ± 59
SO_4^{2-} [mg/l]	17	214 ± 16	59 ± 16
Water type	Mg-Ca-HCO_3	Mg-Ca-HCO_3-SO_4	Mg-HCO_3
δ^2H [‰ VSMOW]	-78.7	-74.7 ± 5.2	-63.4 ± 4.9
$\delta^{18}O$ [‰ VSMOW]	-11.1	-10.7 ± 0.7	-8.6 ± 0.5
$\delta^{13}C_{DIC}$ [‰ VPDB]	-	2.6 ± 0.3	3.6 ± 0.1
$\delta^{34}S_{SO4}$ [‰ VCDT]	-	-1.7 ± 3.1	-
SI_Arg log	0.7	1.0	0.7
SI_Cc log	0.9	1.2	0.9
P_{CO2} log	-2.99	-2.4 ± 0.1	-3.1 ± 0.1

The erzbergite formation temperature was determined by means of clumped isotope measurements conducted on a set of aragonite samples taken across the entire Erzberg (Boch et al., 2019) (Table 2). The obtained formation temperatures for the erzbergite range between 0 to 10 °C, signifying a low temperature origin of the erzbergite.

***Table 2**: Erzbergite formation temperatures in °C, revealed by clumped isotope measurement from Boch et al. (2019).*

Sample	T in °C from Δ_{47}
EB1-Cl1	4 ± 3
EB1-Cl2	2 ± 8
EB6-Cl1	3 ± 5
EB7-Cl1	3 ± 7
EB12-Cl1	8 ± 2
EB12-Cl2	9 ± 4
EB21-Cl1	5 ± 4

These existing formation temperatures are supplemented by new clumped isotope measurements of erzbergite and dolomite samples collected from the southern section of the Erzberg, more precisely from the sample 4B (Fig. 3B). Calculated temperatures of erzbergite formation vary from 3.2 to 14.4 °C, whereas the dolomitized layers exhibit formation temperatures between 2.8 to 4.1 °C (dark brown deposits) and between 8.3 to 20.3 °C (light beige deposits), respectively (Table 3; data source: T. Kluge; S. Bernasconi).

***Table 3:** Formation temperatures obtained for erzbergite and adjacent dolomitized sections of dark brown to light beige color, based on clumped isotopes (data source: T. Kluge; S. Bernasconi).*

Sample	T in °C from Δ_{47}
Erzbergite 1	3.2
Erzbergite 2	7.8
Erzbergite 3	14.4
Matrix dolomite (dark layer 1)	2.8
Matrix dolomite (dark layer 2)	4.1
Matrix dolomite (light layer 1)	8.3
Matrix dolomite (light layer 2)	20.3

3. MATERIAL AND ANALYTICAL METHODS

3.1. Field work and sampling

Field work (geological mapping and sampling) was carried out in November 2016. Hand-size samples were collected from a cataclastic (fault) zone from the southwestern part of the Erzberg, the so-called “Schuchart-Etage” (Fig. 1D). For petrographic, mineralogical, isotopic, major/minor/trace elemental and (micro)structural characterization of the mostly calcareous sedimentary rocks non-oriented specimens (15, in total) were gathered. The sample collection comprises of light beige and brownish carbonate cataclasites, (3C, 4B: sample with subsamples 1 to 13, EB9) which are referred to as type 1 and type 2, respectively, based on optical appearances (i.e. color) (Fig. 3). For comparison, samples from the adjacent erzbergite, the Devonian host rock and the iron ore have been taken (Fig. 1D and 3). Polished thick sections (produced with a thickness of ~ 50 µm) were prepared from these rocks to study the depositional facies as well as possible diagenetic alteration by optical microscopy and electron microprobe analysis. The classification schemes and the nomenclature of Sibley and Gregg (1987); Tucker and Wright (1990); Reinhold (1998) and Flügel (2004) were used for the description and interpretation of the main types of limestone and dolostone microfacies and rock textures.

3.2. X-ray diffraction

X-ray diffraction (XRD) was used for mineral identification and quantification of 13 bulk samples. Samples were first milled for 7-10 minutes in a ball mill to gain a finely-ground powder and then homogenized further by hand in an agate-mill. The top loading technique was used for sample preparation to obtain random orientation of the particles. XRD analyses were carried out on a PANalytical X´Pert PRO diffractometer fitted with a Co-target tube and operated at 40 kV and 40 mA. This device is equipped with a Scientific X´Celerator detector, 0.5° antiscattering and divergence slits, spinner stage, primary and secondary soller and an automatic sample changer. Samples were analyzed over the range of 4-85° 2θ with a step size of 0.008° 2θ/s and a count time of 40 s/step. The quantitative, mineralogical composition of the bulk samples was determined by Rietveld analyses of the XRD patterns using the PANalytical X´Pert HighScore Plus Software and a pdf-4 database.

Dolomite stoichiometry was calculated using the linear expression 1 (Royce et al., 1971; Lumsden and Chimahusky, 1980), where the position of the $d_{(104)}$-peak (in Å) of dolomite is related to its chemical composition:

$$mol\%\ CaCO_3 = 333.33 \cdot d_{(104)} - 911.99 \quad (1)$$

In the present study, the sample displacement was fixed to the peak position of quartz or, alternatively, to aragonite (for samples that contained no quartz) to yield an analytical error below ~1.5 mol% $CaCO_3$ in dolomite.

The degree of cation order (R) in dolomite was calculated using equation 2 (Füchtbauer and Goldschmidt, 1965; Füchtbauer and Richter, 1988; Hardy and Tucker, 1988):

$$R = I\ d_{(015)} / I\ d_{(110)} \quad (2)$$

where (I) represents the diffracted intensities of the $d_{(015)}$- and $d_{(110)}$-reflections of dolomite in counts per second (cps). This technique is semi-quantitative. Due to the different orientation and size of the dolomite particles, the overall error is ± 5%.

3.3. Electron microprobe analyses

The rock textures, microfabrics and geochemical compositions of dolomite-, calcite- and aragonite-bearing samples from the Erzberg were investigated by electron microprobe analyses (EMPA) conducted on a Jeol JXA8200 SuperProbe Electron Probe Microanalyzer (EMPA) at the Montanuniversity of Leoben (Austria) as well as on a Jeol JXA8230 SuperProbe Electron Probe Microanalyzer (EPMA) at the Karl-Franzens-University Graz. The analytical conditions during wavelength-dispersive X-ray spectroscopy (WDXS) analyses were adjusted to 15 keV accelerating voltage, 0.5-3.0 nA beam current and defocused beam, ~0.5-3.0 µm in size, for single-spot analyses of dolomite, aragonite and calcite, respectively. For the quantification of the geochemical data, standardization against natural and synthetic crystals was implemented and included the following elements with characteristic spectral lines: Ca-Kα and Mg-Kα (dolomite), Fe-Kα (almandine), Mn-Kα (rhodonite), Sr-Lα and S-Kα (celestine) and Na-Kα (albite). Counting times of 20-40 s on peak and 10 s on the background position on each side of the Ca, Mg, Fe, Mn, Na, Sr and S peaks were used. Only results with an analytical error of ± 5 % were considered in later discussions. Element distribution maps of 1024 × 1024 pixel resolution were acquired using a focused beam, ~1 µm in size, 15 keV accelerating voltage, 30 nA beam current and a dwell time of 12 ms/step.

3.4. X-ray fluorescence

X-ray fluorescence (XRF) spectroscopy was performed to study the major and minor elemental composition of the samples. Therefore, powdered sample material was dried in a compartment drier at 105 °C overnight. Afterwards, 3 g of sample powder was transferred into a porcelain crucible, glowed for 1 hour at 1050 °C to release volatiles (e.g. H_2O and CO_2) and then the loss on ignition (LOI) was determined by gravimetric analysis. Subsequently, the residue was homogenized. About 1 g of sample and 6 g of di-lithiumtetraborate were mixed in an agate-mortar. The homogenized mixture was conveyed into a platinum crucible and then fused in an automatic fusion device (Perl'X PANAlytical) at 1150 °C for 12 min. The resulting glass tablets were analyzed with a wavelength dispersive X-ray spectrometer (PW 2404). The analytical error was determined to be ± 1 wt.% for the major elements.

3.5. Inductively coupled plasma optical emission spectroscopy

Major, minor and trace elemental compositions of the acid-soluble fraction of bulk rock samples (i.e. carbonates and labile Fe-oxyhydrates) were obtained by inductively coupled plasma optical emission spectroscopy (ICP-OES) analyses performed on a PerkinElmer Optima 8300. To ensure complete digestion of the barely soluble Ca-Mg carbonates (i.e. dolomite), 5 mg of sample powder was reacted with ~45 g of 6 % HNO_3 (utilizing HNO_3 of suprapure grade) for 12 h in an ultrasonic bath at 70°C. Subsequently, the solid residue was removed by filtration through 0.45 µm cellulose acetate filters. The analytical precision (2σ, 3 replicates) of the ICP-OES analyses is ± 2 % for major and minor elements and ± 3 % for trace elements, respectively, based on replicate measurements of NIST 1640a and SWS-2 batch standards.

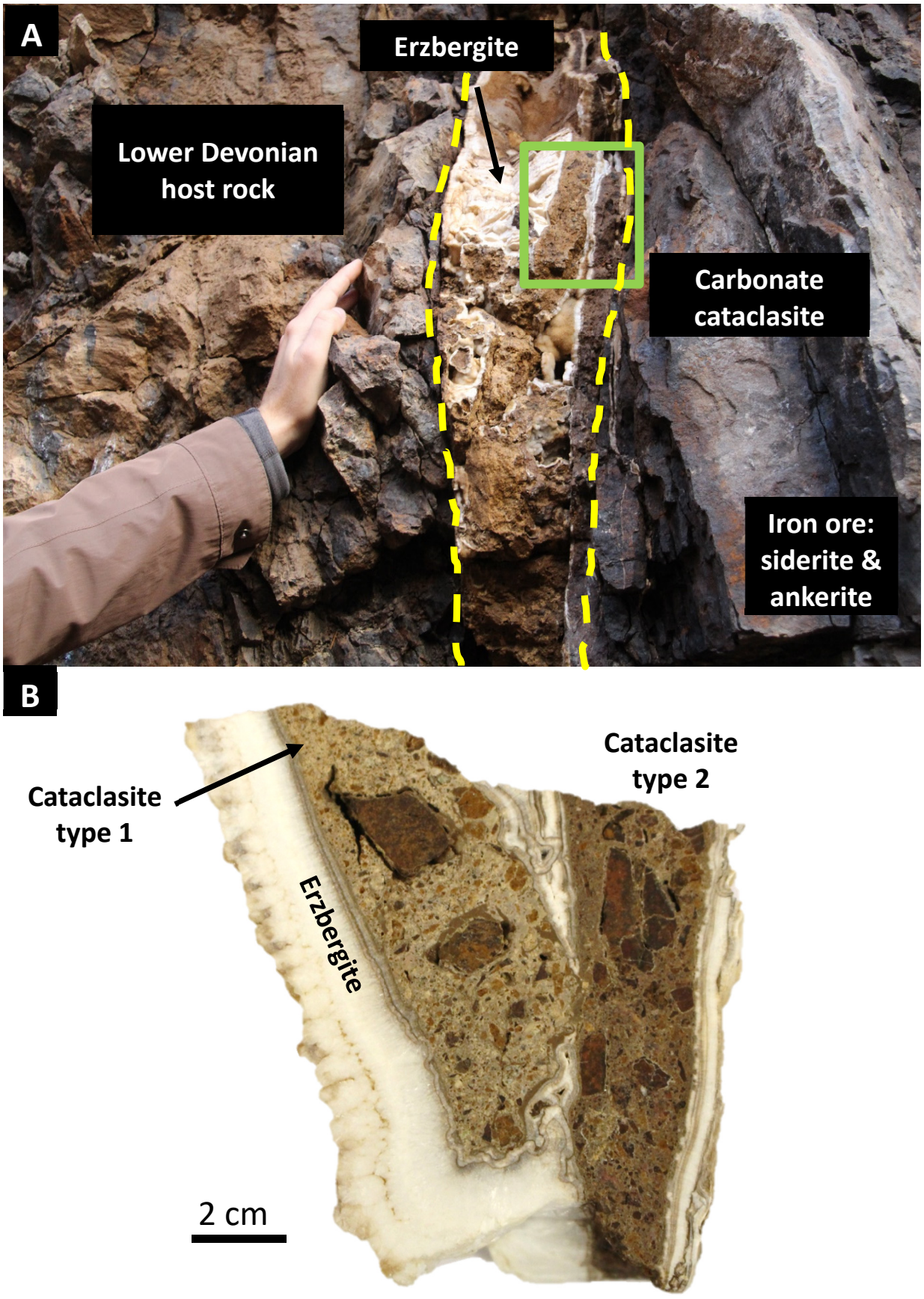

***Fig. 3**: (A) Sampling of the cataclastic zone from the Schuchart-Etage, SW Erzberg. Note the occurrence of whitish erzbergite (aragonite and calcite) and intercalated (dolomite-rich) cataclastic material. (B) Close-up of the sample showing the light beige cataclasite type 1 and dark brown cataclasite type 2. Note that the two cataclasite types are sandwiched by erzbergite deposits.*

3.6. Stable oxygen and carbon isotopes

The oxygen and carbon isotopic composition of dolomite- and erzbergite-containing samples was analyzed with a ThermoFisher Scientific Gasbench II connected to a ThermoFinnigan DELTAplus XP mass spectrometer at the stable isotope laboratory of the JR-AquaConSol GmbH (Graz, Austria). A DREMEL 3000 driller, equipped with a tungsten carbide drill, was used for spotty sampling of the specimens (i.e. the dolomite matrix as well as pure erzbergite were selectively probed). Prior to the stable isotope analyses by continuous-flow isotopic ratio mass spectrometric measurements, about 200 to 600 µg of the sample was transferred into pre-purified sample vials, following injection of highly concentrated phosphoric acid and reaction for 2 h at 70 °C. The obtained values for carbon ($\delta^{13}C$) and oxygen ($\delta^{18}O$) isotopes are given in terms of delta notation and are declared as deviation from the international Vienna-Pee Dee Formation belemnite (V-PDB) standard in per mil (‰). The analytical reproducibility was better than ± 0.1 ‰ for $\delta^{13}C$ and $\delta^{18}O$ analyses, respectively.

3.7. Magnesium isotopes

Separation and subsequent purification of Mg from digested Ca-Mg carbonates (4 in total) and from two fluid samples taken from the southern section of the Erzberg (Boch et al., 2019) were achieved by using two-step ion exchange chemistry (HNO_3 and HCl) and following the protocol of Wombacher et al. (2009). Briefly, a small amount of solid sample (ca. 100 mg) was leached out with 4 M HNO_3 at 80 °C. The fluids were used as received. In a first step quantitative separation of Ca and other bivalent cations from the two sets of liquid samples was realized by passing the respective solutions through individual columns (length: 5 cm, diameter: 0.5 mm, reservoir: 5 ml, BioRad AG50W-X12 resin: ~1 ml, load: 2 M HNO_3). The Mg recovery was tested by running a MERCK standard solution (containing 10 µg/ml of Mg, Ca, Sr, Zn, Fe, Ti and Cu) over the same columns. The collected samples were evaporated to dryness and re-dissolved in 1 ml 0.4 M HCl. In the second step, the samples were loaded to the columns, followed by washing with 30 ml 0.4 M HCl, rinsing with 1 ml 1 M HCl and recovery of the Mg fraction in another 12 ml 1 M HCl. The remaining, purified Mg sample was again evaporated to dryness at 90 °C and re-dissolved in 0.45 M HNO_3.

Prior to the Mg isotope analysis all analytes and standard solutions were diluted with 0.45 M HNO_3 to yield a target Mg concentration of about 0.5 µg/ml (e.g., ± 15 % of the standard to minimize potential isobaric interferences from matrices (Galy et al., 2001). Subsequently, Mg isotope ratios were measured on a Nu Plasma 2 multi-collector inductively coupled plasma mass spectrometer (MC-ICP-MS) using the standard sample bracketing technique (SSB) and applying a DSM3 reference solution to correct for instrumental mass bias (Galy et al., 2003).

Furthermore, two international standards (CAM1 and JDO1) were measured as quality checks. The Mg isotopic ratios are reported in terms of δ-notation, relative to the DSM3 reference material, where $\delta^{26}Mg$ and $\delta^{25}Mg$ refer to the ratios of $^{26}Mg/^{24}Mg$ and $^{25}Mg/^{24}Mg$, respectively. The analytical precision (2δ, 5 replicates) of the $\delta^{26}Mg$ and $\delta^{25}Mg$ isotope analyses was determined to be ± 0.2 ‰. However, from the obtained $^{26}Mg/^{24}Mg$ and $^{25}Mg/^{24}Mg$ ratios it can be inferred that the Mg separation was biased by matrix effects for that an impure resin was used for the separation. For example, the JDo-1 standard and all dolomite were significantly away from the ideal fractionation line. For this reason, these data are not taken into further consideration but are listed in the appendix.

3.8. Hydrogeochemical modeling

Hydrogeochemical modeling of modern surface and fracture waters from the Erzberg (Fig. 1C) was carried out using the PHREEQC computer code (version 2.18) and the implemented wateq4f.dat database (Parkhurst and Appelo, 2013). Ion charge balances, ionic activities, ionic strength, aqueous speciation, internal CO_2 partial pressure (P_{CO2}) and mineral saturation indices (SI) were calculated at the given pH and temperature (Table 1). A characteristic parameter for dissolution or precipitation of a mineral phase from a solution is the saturation index defined by equation 3:

$$SI = log \frac{IAP}{K_{sp}} \quad (3)$$

where IAP is the ion activity product and K_{sp} represents the solubility product (in equilibrium) of the mineral. Three different ranges of values can be distinguished: (i) SI = 0: the mineral phase is in thermodynamically equilibrium with the solution; (ii) SI < 0: dissolution of the mineral phase occurs and (iii) SI > 0: indicates mineral precipitation.

4. RESULTS

4.1. Petrographic description of carbonate vein infillings

Microscopic observations of polished thick sections using light and transmitted light microscopy revealed an alternating sequence of Ca-Mg carbonate infillings within fractures and veins at the Erzberg (Fig. 4). These authigenic Ca-Mg carbonate deposits generally consist of fine-grained, matrix-supported (dolomite-containing) cataclasite horizons of variable thickness (mm- to cm-scale), which are sandwiched by massive aragonite layers (erzbergite). Specifically, the following deposits can be distinguished in thick sections (Fig. 4):

1) Carbonate cataclasite: Based on color of the matrix containing dolomite, two different types of cataclasites can be distinguished: type-1 is light brown to beige and type-2 is more brownish due to a generally higher content of finely dispersed Fe-oxyhydrates in the matrix (Fig. 3 B). Basically, both cataclasites have a matrix-supported texture, as no grain to grain boundaries were visible in the investigated sections. Furthermore, neither grading (fining upwards or coarsening upwards sequences) nor special orientation (i.e. readjustment textures) of the components (clasts) was recognizable. The clasts have a reddish-brown color, are mainly composed of Fe-oxyhydrates and minor quartz, though the presence of trace amounts of reworked iron ore (ankerite and siderite) cannot be fully ruled out. Secondary veins, pervasive fractures and associated Ca-carbonate fillings of aragonite and calcite spar are very common in the carbonate cataclasites (Fig. 4: C, D).

2) Erzbergite: Snow white to beige laminations, ranging from (sub)-millimeter to centimeter scale, are characteristic for the erzbergite (Fig. 4: A, B). The individual laminae consist of radial-shaped aragonite needles, which form irregular to patchy intervals within the erzbergite. Different growth directions of the aragonite crystals can be frequently observed. The aragonite crystals have either an acicular or a normal fibrous form and show undulatory light extinction. Within the aragonite layers, subhedral to euhedral (i.e. rhombohedral) calcite crystals of few µm-size occur, which have likely formed during spatial recrystallization of the aragonite (Fig. 4: A, B). These calcite crystals are referred to as calcite spar. Repeatedly, the aragonite deposits are interrupted by very thin and reddish-brown laminae of Fe-oxyhydroxides, which may indicate growth interruptions due to changes in the precipitation regime, according to Boch et al. (2019).

3) Dolomite:

In both types of carbonate cataclasites the matrix consists of matrix dolomite that is indistinguishable from each other regarding crystal size and shape, occurrence and fabric: the individual grains are between 5 to 20 µm in size, have a subhedral (planar-s) shape, form a pervasive fabric and occur in completely dolomitized areas. Very rarely, partly dissolved aragonite needles are preserved within the matrix dolomite (for further characterization of the dolomite the reader is referred to the section on EMPA results) (Fig. 4: C, D).

In addition, white to beige coatings and fracture fillings of dolomite consistently appear around and in Fe-oxyhydroxide clasts (mainly around reworked and partly broken Fe-oxyhydroxide grains) as well as in fractures throughout the carbonate cataclasite. Therefore, it seems that the occurrence of dolomite is restricted to stylolites within and around clasts or along fractures penetrating the carbonate cataclasite. Individual dolomite crystals are relatively coarse (up to several hundreds of µm in largest dimension), have a subhedral to rhombohedral shape and consist of pure dolomite. These so-called dolomite spheroids have a fabric-selective to pervasive fabric. No remains of calcite and/or aragonite matrix are preserved within this dolomite, which indicates almost complete dolomitization (Fig. 4: E, F).

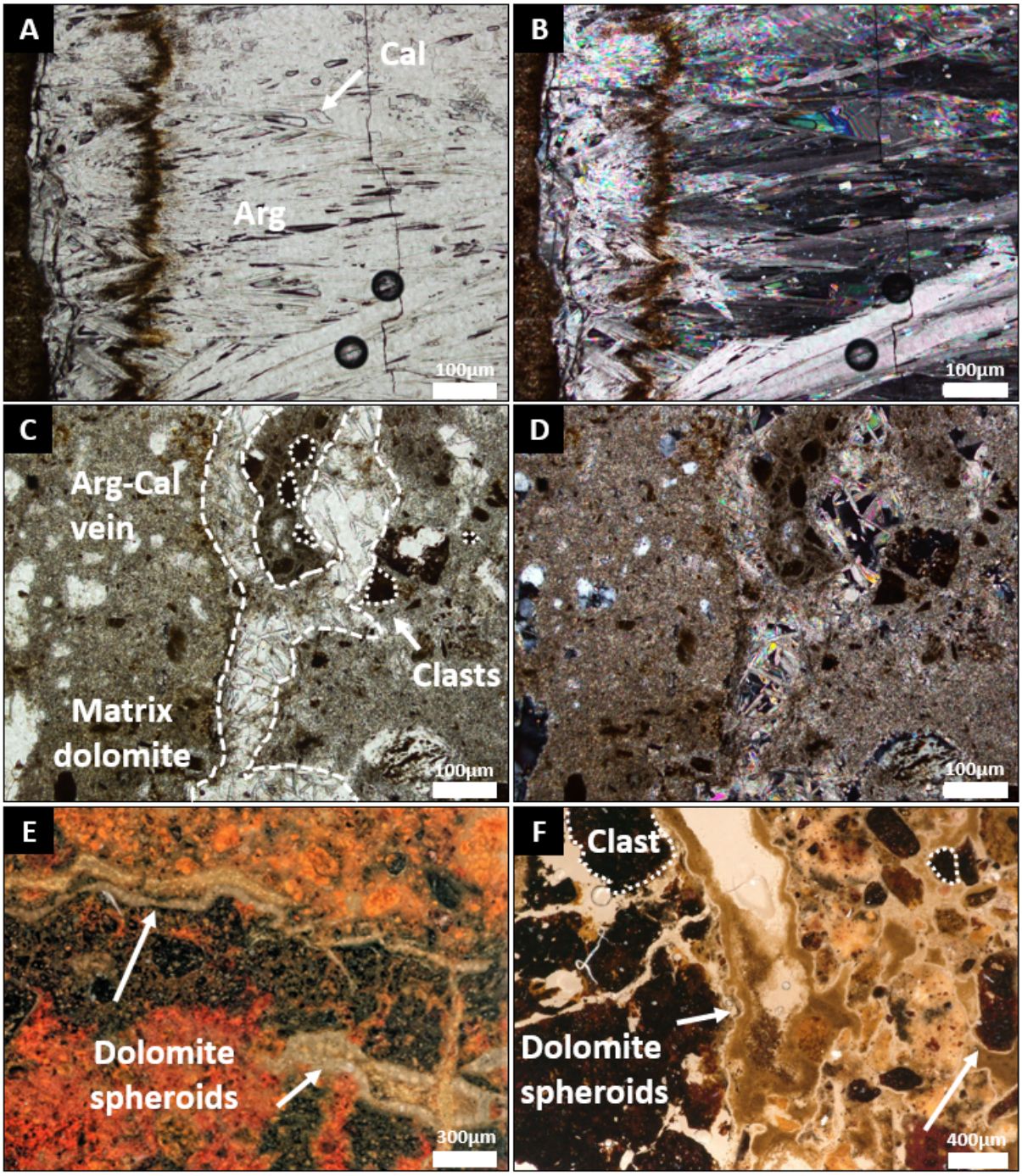

Fig. 4: *Photomicrographs of polished thick sections (crossed nicols on the right) showing (A-B) laminated successions of embedded needle-shaped, radiating aragonite (Arg) and blocky calcite spar (Cal). (C-D) Matrix dolomite from the light beige (type 1) carbonate cataclasite. (E-F) light microscope images of dolomite spheroids (E, F) from the dark brown (type 2) carbonate cataclasite. The reddish-brown clasts (C, F) consist of aggregated Fe-(oxy)hydroxides (e.g. goethite and hematite).*

4.2. Mineralogical observations

Exemplary examination of the obtained XRD pattern for the carbonate cataclasites types 1 + 2 and their analyzed mineral phases are summarized in Fig. 5. Furthermore, Fig. 6 shows the two important dolomite peaks (d_{105} and d_{110}) that are necessary for the calculation of the cation ordering degree (COD). Changes in the mineralogical composition across the erzbergite deposits versus carbonate cataclasites type 1 and type 2 from the Erzberg are presented in Fig. 7A-B.

Nearly pure aragonite (± low-Mg calcite, LMC) is found in samples representing the erzbergite. Type 1 of the carbonate cataclasites consist mainly of dolomite (70-86 wt.%), in addition to minor amounts of Fe-oxyhydroxides (2-7 wt.%), quartz (4-5 wt.%), muscovite (3-7 wt.%), LMC (2-7 wt.%) and aragonite (2-13 wt.%). In contrast, type 2 of the carbonate cataclasites is composed of comparably lower proportions of dolomite (68-78 wt.%), LMC (2-4 wt.%) and aragonite (1-4 wt.%) and higher amounts of Fe-oxyhydroxides (10-18 wt.%), quartz (~5 wt.%) and muscovite (2-6 wt.%). From these data it becomes clear that the darker color of this carbonate cataclasite type 2 is due to the higher Fe-oxyhydroxide content, which corroborates the results obtained from optical microscopy of thick sections. In conjunction with the transmitted light microscope images, it can be inferred that the small amounts of calcite and aragonite correspond to secondary vein infillings (cf. Fig. 4: C-D). Samples 5 and 6 represent a mixture of erzbergite and adjacent carbonate cataclasites, thus they have a high aragonite and dolomite content (cf. Fig. 7B), but a low Fe-oxyhydroxide, quartz and muscovite content. Both carbonate cataclasite types contain low amounts of erzbergite, which is shown by the erzbergite to dolomite ratio in Fig. 7C.

The Ca-content in dolomite was determined as 51 to 54 mol% $CaCO_3$, which is typical for sedimentary Ca-excess dolomites (Fig. 7C). Insignificant differences in stoichiometry were recognized for the matrix dolomites and dolomite spheroids from the carbonate cataclasites by XRD. The calculated COD of dolomite varied between 0.35 (dark brown type 2) and 0.25 (light beige type 1) (Fig. 6), which is very common for dolomites formed at low temperatures. It is worthy to note that a clear separation between dolomite and ankerite was not possible (i.e. trace amounts of ankerite could be present in the samples) due to the overlapping of the $d_{(104)}$ reflections of dolomite (2.91-2.88 Å) and ankerite (~2.90 Å). However, the existence of siderite can be excluded, because the main peak of siderite ($d_{(104)}$ at 2.79 Å) was absent.

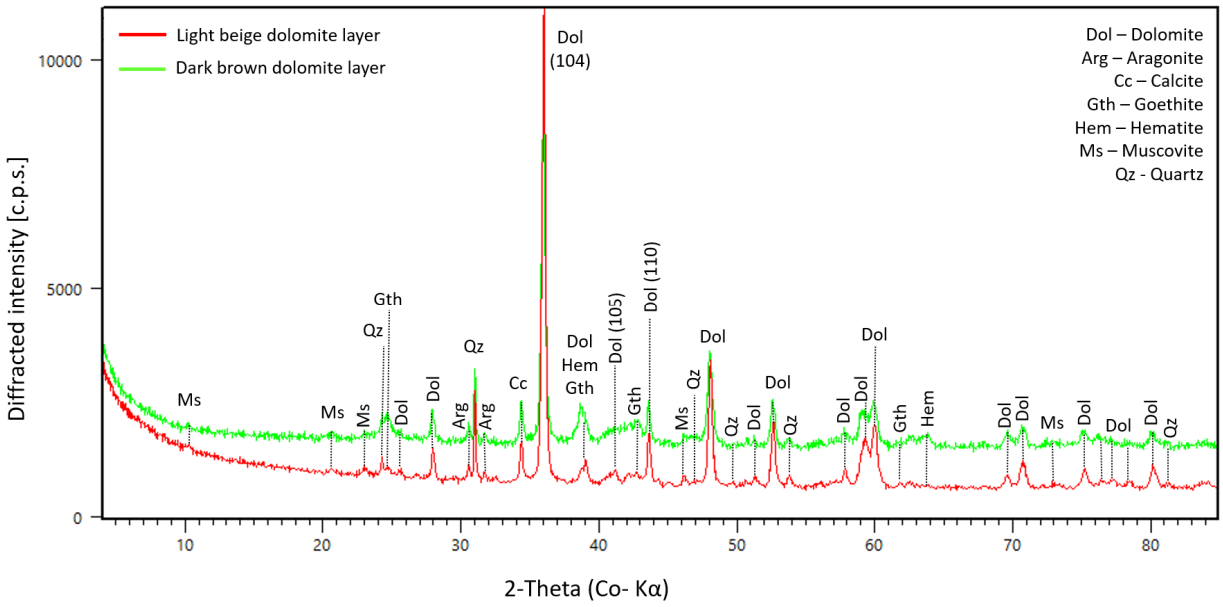

***Fig. 5**: XRD patterns comparing the mineralogy of the light beige dolomite layer (red) and the dark brown dolomite layer (green). In both layers the carbonates dolomite, aragonite and calcite as well as Fe-(oxy)hydroxides (goethite and hematite), muscovite and quartz have been identified.*

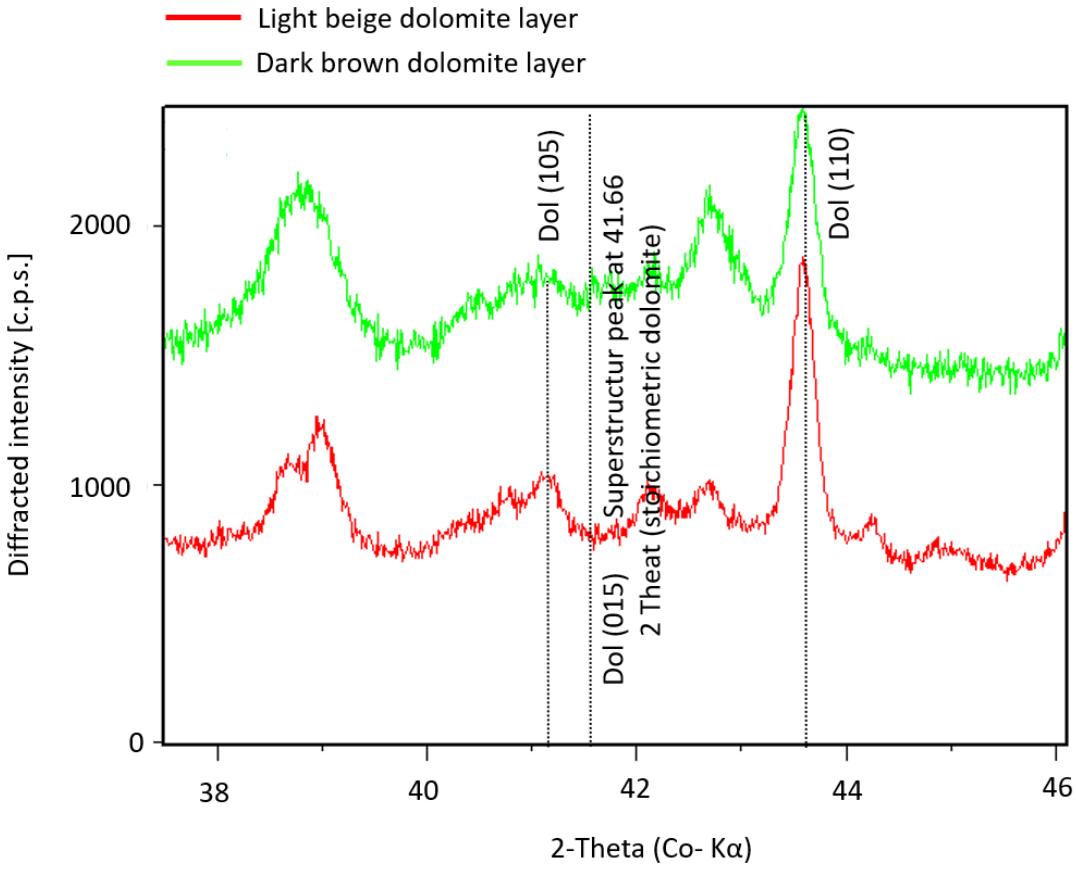

***Fig. 6**: XRD pattern showing the region between 38-46 °2θ. Both diffractograms comprehend the superstructure peak d_{105} at 41.2 °2θ. The superstructure peak for ideal dolomite normally lies at 41.66 °2θ. To calculate the cation ordering degree the intensity ratio of the d_{105} peak to the d_{110} peak is used.*

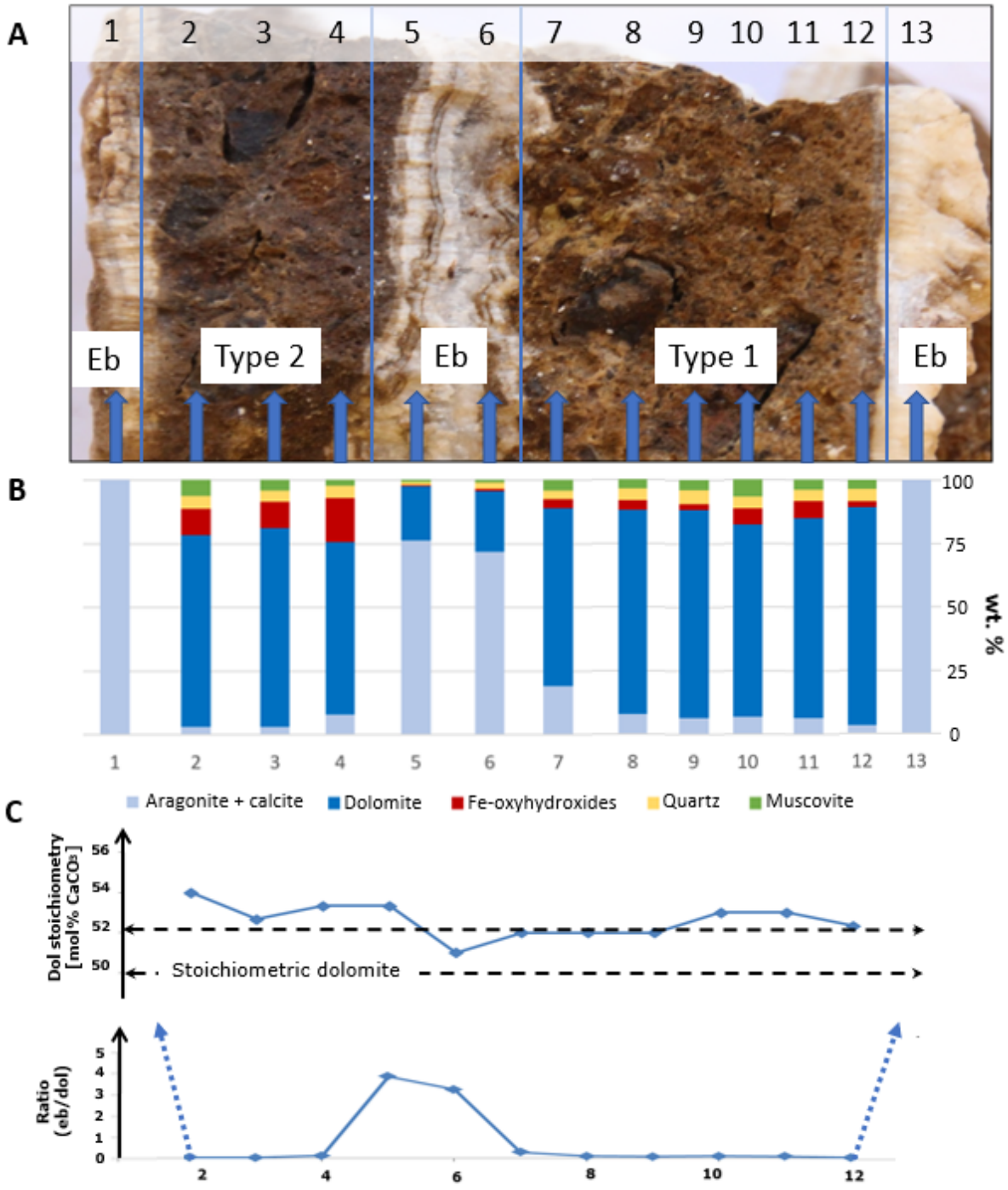

***Fig. 7**: (A) Mineralogical composition across the sequence of authigenic Mg-Ca-carbonates from the carbonate cataclasites at the Erzberg. Delineated lines (blue) separate the erzbergite from carbonate cataclasites type 1 and 2. Arrows mark the position of samples taken for XRD analyses. (B) Quantitative phase composition (in wt.%) of pure erzbergite (sample 1+13), carbonate cataclasite type 2 (sample 2-4), carbonate cataclasite type 1 (sample 7-12) and intergrowth succession (sample 5-6). Note that for this figure aragonite and calcite were gathered as erzbergite, and that matrix dolomite and dolomite spheroids as well as goethite and hematite have been summed up as dolomite and Fe-oxyhydroxides, respectively. (C) Changes in dolomite stoichiometry and dolomite/erzbergite ratio across the investigated profile.*

4.3. Geochemistry of carbonate deposits

Bulk rock composition

XRF results (Fig. 8) of the investigated 13 bulk samples show that erzbergite samples mainly consists of CaO, corresponding to the $CaCO_3$ polymorphs aragonite and calcite. Opposed to this, carbonate cataclasites type 1 and 2 additionally persist of MgO ($MgCO_3$), which indicates the existence of dolomite. Surprisingly high Fe_2O_3 contents were measured across the Ca-Mg carbonate vein infillings, much higher than expected and calculated by XRD and ICP-OES analyses (see below). The reasons for this remain unclear. Maybe the fact that no Fe-carbonate standard was considered has biased the XRF results. Apart from this, carbonate cataclasite type 2 exhibits higher Fe_2O_3 concentrations (20-24 wt.%) than carbonate cataclasite type 1 (6-11 wt.% Fe_2O_3), which in turn explains the darker color of the carbonate cataclasite type 2 (Fig. 8). Again, samples 5 and 6 represent a mixture of erzbergite and carbonate cataclasites. A separation between erzbergite and carbonate cataclasites type 1 and type 2 is shown in the plot of MgO versus CaO (Fig. 8). Minor proportions of SiO_2 and Al_2O_3 belong to silicate phases (clay minerals and quartz). MnO is negligible. The high LOI contents correspond to carbonates (erzbergite and dolomite) and subordinate phyllosilicates.

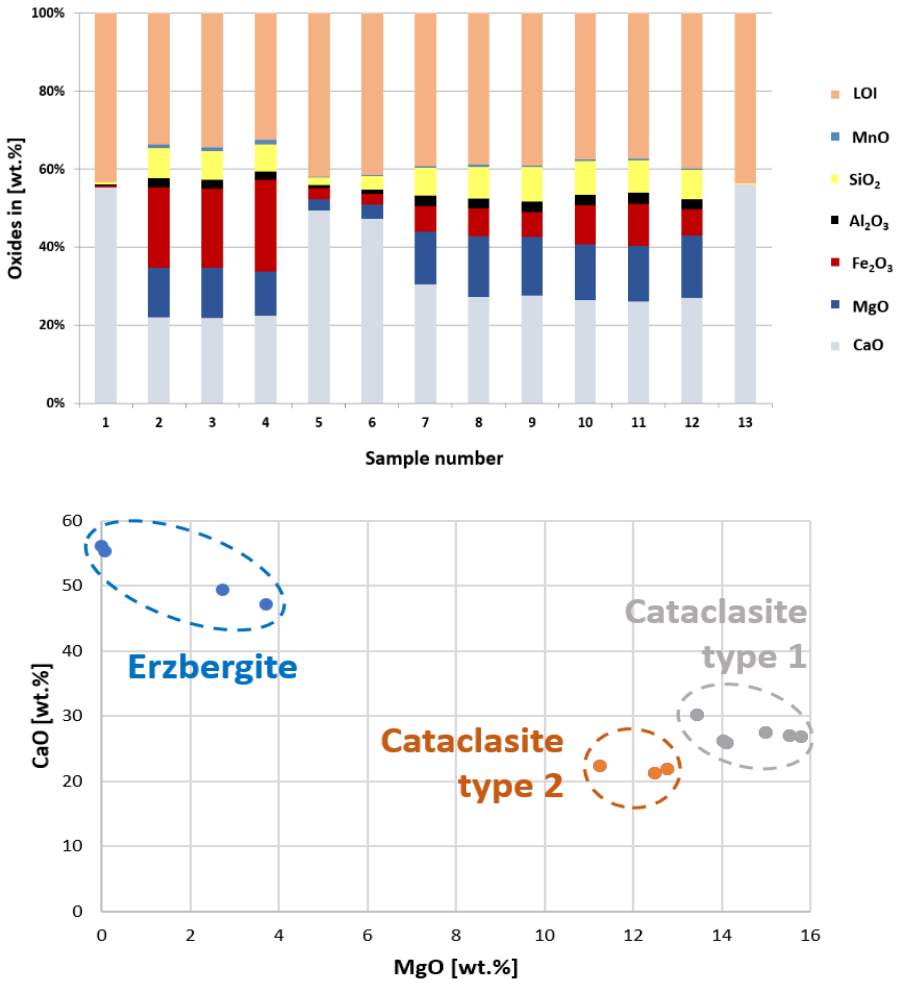

***Fig. 8**: Upper figure: XRF results of the 13 bulk sample shown in Figure 7A. Variations in CaO and MgO contents correspond to different rock types: erzbergite, carbonate cataclasite type 1 and type 2 or admixtures. Lower figure: Cross-plot of MgO vs. CaO showing domains of erzbergite and carbonate cataclasite samples.*

Carbonate fraction

Based on ICP-OES results, the bulk samples can be divided into three groups: 1) erzbergite, 2) carbonate cataclasite type 1 and 3) carbonate cataclasite type 2 (Table 4) (samples 5+6 form mixtures of the mentioned groups and are listed in the appendix). Main differences between these groups can be seen by the element concentrations of Ca and Mg. Erzbergite samples contain high amounts of Ca (34 ± 2.2 wt.%) and less Mg (1 ± 0.9 wt.%). In contrast, carbonate cataclasite type 1 comprises of 17 ± 0.2 wt.% of Ca and 8 ± 0.4 wt.% of Mg, while carbonate cataclasite type 2 exhibits 14 ± 0.9 wt.% of Ca and 7 ± 0.6 wt.% of Mg. The analyzed Fe content of the erzbergite samples amounts to 1 ± 0.9 wt.%, whereas carbonate cataclasite type 1 and type 2 comprise 5 ± 0.9 wt.% and 11 ± 0.9 wt.% of Fe. Measured Na concentrations are very low in all samples (erzbergite: < 10 to 14 ppm; carbonate cataclasite type 1: < 10 to 45 ppm; carbonate cataclasite type 2: < 10 ppm). The same can be stated for the Sr values (erzbergite: 79 ± 3 ppm; carbonate cataclasite type 1: 22 ± 3 ppm; carbonate cataclasite type 2: 16 ± 5 ppm). Relatively high Mn concentrations were measured in all sample types, particularly in the carbonate cataclasite samples (carbonate cataclasite type 1: 2773 ± 262 ppm; carbonate cataclasite type 2: 4631 ± 315 ppm versus erzbergite: 794 ± 659 ppm).

***Table 4**: Excerpt of ICP-OES data (cf. appendix): Minima, maxima and mean concentration values with standard deviations (2σ) are reported for the following elements: Na, Sr, Fe, Mn, Ca and Mg. The Ca:Mg molar ratio allows distinguishing between erzbergite, carbonate cataclasite type 1 and carbonate cataclasite type 2.*

		Ca [wt. %]	Mg [wt. %]	Fe [wt. %]	Na [ppm]	Sr [ppm]	Mn [ppm]	Ca:Mg [molar]
Erzbergite (n=4)	Min.	31	0	0	<10	74	20	9.6
	Max.	37	2	2	14	82	1570	1874
	Mean	34 ± 2.2	1 ± 0.9	1 ± 0.9	-	79 ± 3.2	794 ± 659	612
Cataclasite type 1 (n=6)	Min.	18	7	4	<10	18	2254	1.3
	Max.	21	9	6	45	32	3198	1.8
	Mean	19 ± 0.2	8 ± 0.4	5 ± 0.9	-	22 ± 2.8	2773 ± 262	1.4
Cataclasite type 2 (n=3)	Min.	14	6	11	<10	14	4332	1.3
	Max.	15	7	13	<10	20	4970	1.5
	Mean	14 ± 0.9	7 ± 0.6	11 ± 0.9	<10	16 ± 4.6	4631 ± 315	1.4

4.4. Microstructural, chemical observations and dolomite classification

The investigation of thick sections (containing both carbonate cataclasites) via EMPA enabled the following dolomite classification based on distinguishable microstructure and different chemical composition.

Dolomite spheroids:

This dolomite type is texture-selective to pervasive and shows concentric zonation patterns with Ca-rich cores and Mg-rich rims (Fig. 9: B, D). Individual dolomite crystals are arranged in mosaic structures, which is typical for spheroidal dolomite. This dolomite is exclusively found in former fissures or fractures (preferentially in reworked, broken Fe-oxyhydroxide grains) within both carbonate cataclasites (Fig. 9: A, B, D). This dolomite type consists of agglomerated dolomite grains with sizes up to several 100 µm, although the individual crystals have a subhedral to rhombohedral form. The absence of calcite and aragonite precursors within the dolomite spheroids suggests that dolomitization is almost complete. Overall, spheroidal dolomite amounts to about 5 vol.% of the total dolomitized rock volume. Dolomite stoichiometry varies in the range of 44-56 mol% $CaCO_3$ (mean: 52 ± 3 mol% $CaCO_3$; n = 103) (Table 5; Fig. 9 E). Elemental distribution maps confirm that the spheroidal dolomite shows zonation patterns, e.g., having higher Mg concentrations in the outer parts (rim structure) of the dolomite crystals, while Ca is relatively enriched in the inner (core) parts (Fig. 10: A, B).

Matrix dolomite:

Matrix dolomite is composed of unimodal, fine-grained (~10 µm in size, on average) dolomite crystals, which have a subhedral (planar s-type) crystal shape. This dolomite type is matrix-replaced (Fig. 9 C). Element distribution mappings of Mg and Ca indicate a homogenous composition of the matrix dolomite, i.e. Ca and Mg are evenly distributed across individual dolomite crystals (Fig. 10 C). Aragonite needles are partly preserved within pore space of the dolomitized matrix, but frequently show signs of dissolution and replacement (e.g. aragonite needles are etched and encapsulated by dolomite), suggesting that aragonite is progressively replaced during dolomitization. Occasionally, matrix dolomite appears as thin coating around and within fissures of clasts (Fig. 9 F). Overgrowth textures of matrix dolomite on preexisting spheroidal dolomite crystals can be observed in rare cases. By far, matrix dolomite is the dominant dolomite type within all investigated samples and builds up about 95 vol.% of the total dolomite volume. The composition of the matrix dolomite ranges from 50-60 mol% $CaCO_3$ (mean: 54 ± 2 mol% $CaCO_3$; n = 179) (Table 5; Fig. 9 E), which is typical for Ca-excess

dolomite. Conspicuous Ca-rich vein fillings percolate the dolomitized sections (Fig. 10 E), suggesting that these calcite and aragonite veins build the last stage in the genetic sequence of Ca-Mg carbonate mineral growth.

Clasts:

As expected, the clasts contain high amounts of Fe and therefore are identified as Fe-oxyhydroxide grains. Most clasts show abundant signs of alteration, such as weathered surfaces, and different stages of transformation (e.g., hematite to goethite reaction, as evidenced by variations in the Fe content over the grains), expressed by so-called “core-rime” structures (Fig. 10 D). The Fe-oxyhydroxide clasts are partly replaced by the two dolomite types and cross-cut by the youngest calcite-aragonite vein system (Fig. 10 E).

Table 5: *Dolomite stoichiometry based on EMPA results. The two different dolomite types: (1) dolomite spheroids and (2) matrix dolomite are displayed, whereby the spheroidal dolomite is more near-stoichiometric than the matrix dolomite.*

	Mg [atom%]			Ca [atom%]		
	Min	Max	**Mean**	Min	Max	**Mean**
Dolomite spheroids (n = 103)	0.43	0.55	**0.48 ± 0.03**	0.44	0.56	**0.52 ± 0.03**
Matrix dolomite (n = 179)	0.39	0.49	**0.45 ± 0.02**	0.50	0.60	**0.54 ± 0.02**

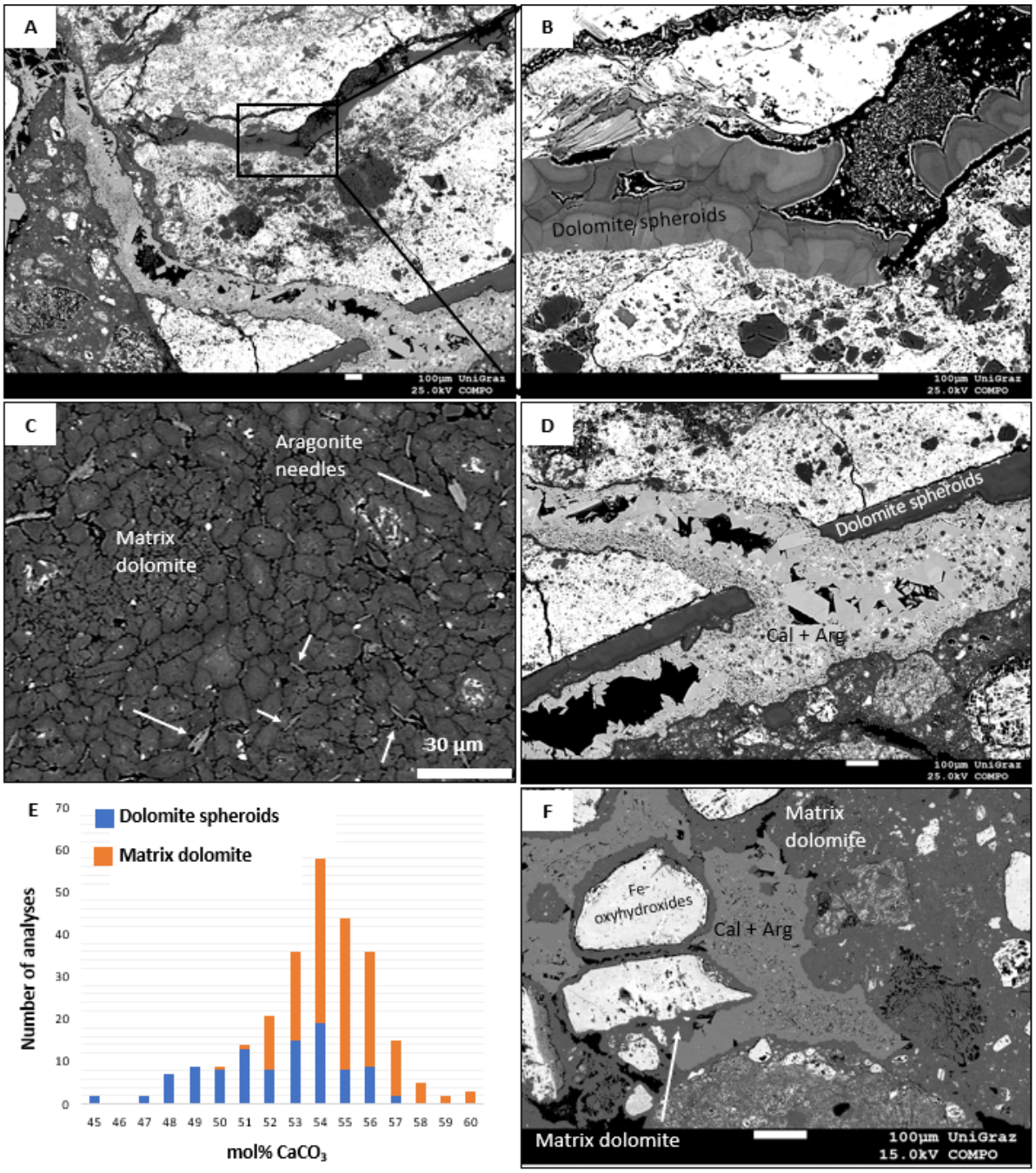

Fig. 9: *Dolomite composition, texture and classification based on EMPA study. (A) Dolomitized section containing calcite/aragonite veins percolating the carbonate matrix. (B) Close-up of A showing zoning and mosaic textures of the spheroidal dolomite (grain size: app. 100 µm). (C) Matrix dolomite (crystal size: app. 10 µm) with interbedded aragonite needles (marked with arrows). (D) Calcite/aragonite veins cross-cutting spheroidal dolomite, dolomitized matrix and Fe-oxyhydroxide grains. (E) Histogram showing the dolomite stoichiometry for both dolomite types, e.g. matrix dolomite is less stoichiometric. (F) Overgrowth features of matrix dolomite on Fe-oxyhydroxide grains.*

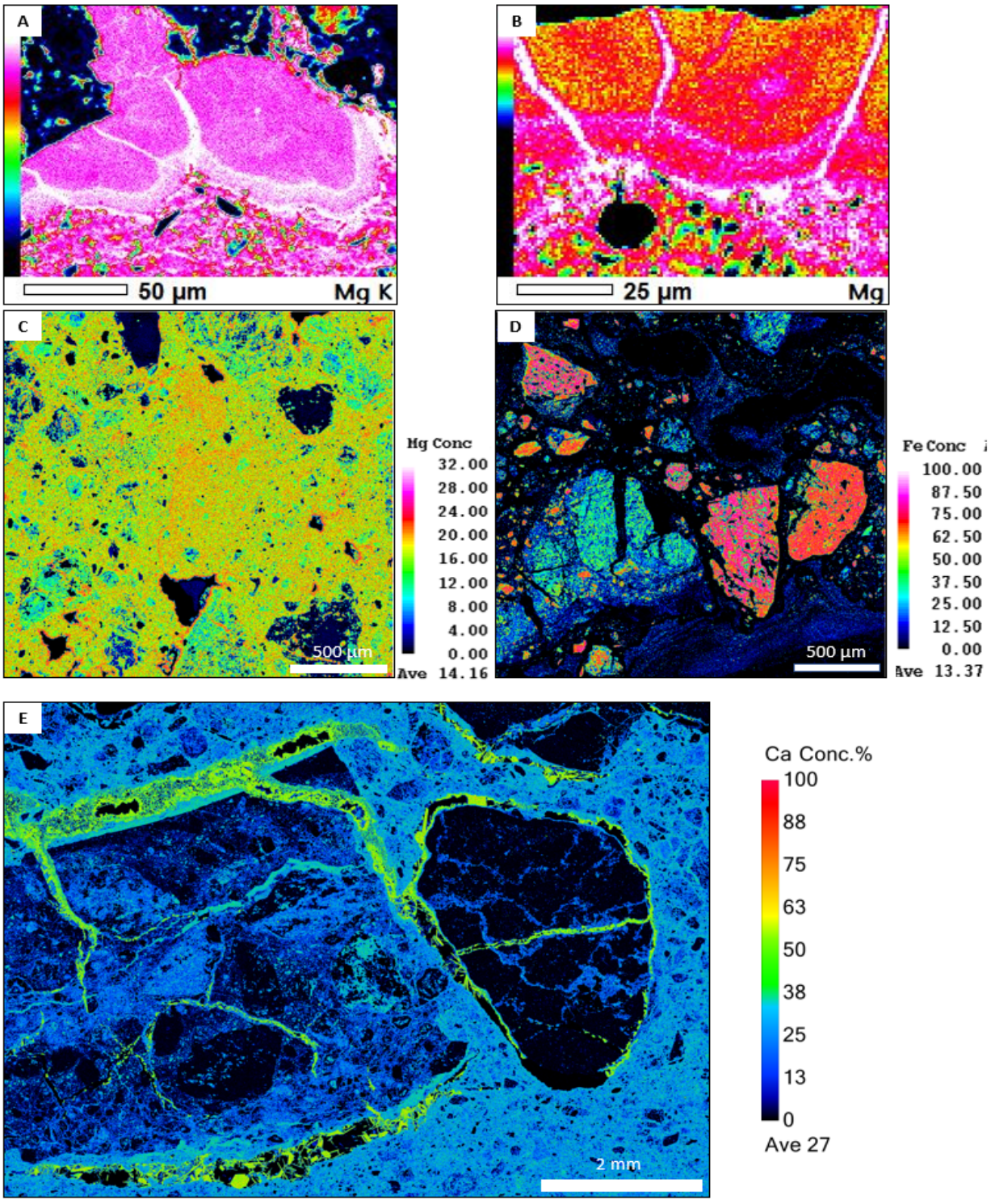

Fig. 10: *Element distribution maps of carbonate cataclasites. (A)+ (B) Mg and Ca distributions across a spheroidal dolomite crystal showing clear zonation patterns. (C) Matrix dolomite reveals a homogenous composition (no zonation patterns) and an even distribution over the entire matrix. (D) Distribution of Fe in clasts. Different types of Fe-oxyhydroxides and rarely ankerite are seen, being partly transformed during weathering (e.g. formation of goethite rims). (E) Ca distribution map displaying calcite-aragonite veins (green) penetrating the dolomitized sections as well as Fe-oxyhydroxide clasts.*

4.5. Isotopic composition of carbonate vein infillings

Carbonate cataclasite type 1 (consist mainly of matrix dolomite) shows $\delta^{13}C$ values from 4.4 to 5.0 ‰ (VPDB; mean: 4.6 ± 0.2 ‰; n = 17) and $\delta^{18}O$ values from -7.2 to -6.0 ‰ (VPDB; mean: -6.4 ± 0.4 ‰; n = 17). Carbonate cataclasite type 2 (comprises more spheroidal dolomite than type 1) yields $\delta^{13}C$ values from 4.2 to 5.3 ‰ (VPDB; mean: 4.8 ± 0.3 ‰; n = 6) and $\delta^{18}O$ values from -8.5 to -6.7 ‰ (VPDB; mean: -7.4 ± 0.5 ‰; n = 6). The erzbergite samples vary in the region from 3.3 to 3.8 ‰ (VPDB; mean: 3.6 ± 0.2 ‰; n = 3) and -10.8 to -7.8 ‰ (VPDB; mean: -8.9 ± 1.3 ‰; n = 3) for $\delta^{13}C$ and $\delta^{18}O$, respectively. Moreover, stable C and O isotopic compositions of the adjacent iron ore reveal generally lower $\delta^{13}C$ (0.3 to -0.8 ‰, VPDB; n = 2) and $\delta^{18}O$ values (-13.5 to -8.6 ‰, VPDB; n = 2), compared to the Ca-Mg carbonate mineralizations. Clasts sampled within the carbonate cataclasite yield $\delta^{13}C$ values of 1.5 to 4.0 ‰ (VPDB; n = 2) and $\delta^{18}O$ values of -9.5 to -9.1 ‰ (VPDB; n = 2). All samples are summarized in a $\delta^{18}O$ versus $\delta^{13}C$ plot (Fig. 11), that contains comparison samples of erzbergite, different host rocks and speleothem carbonates.

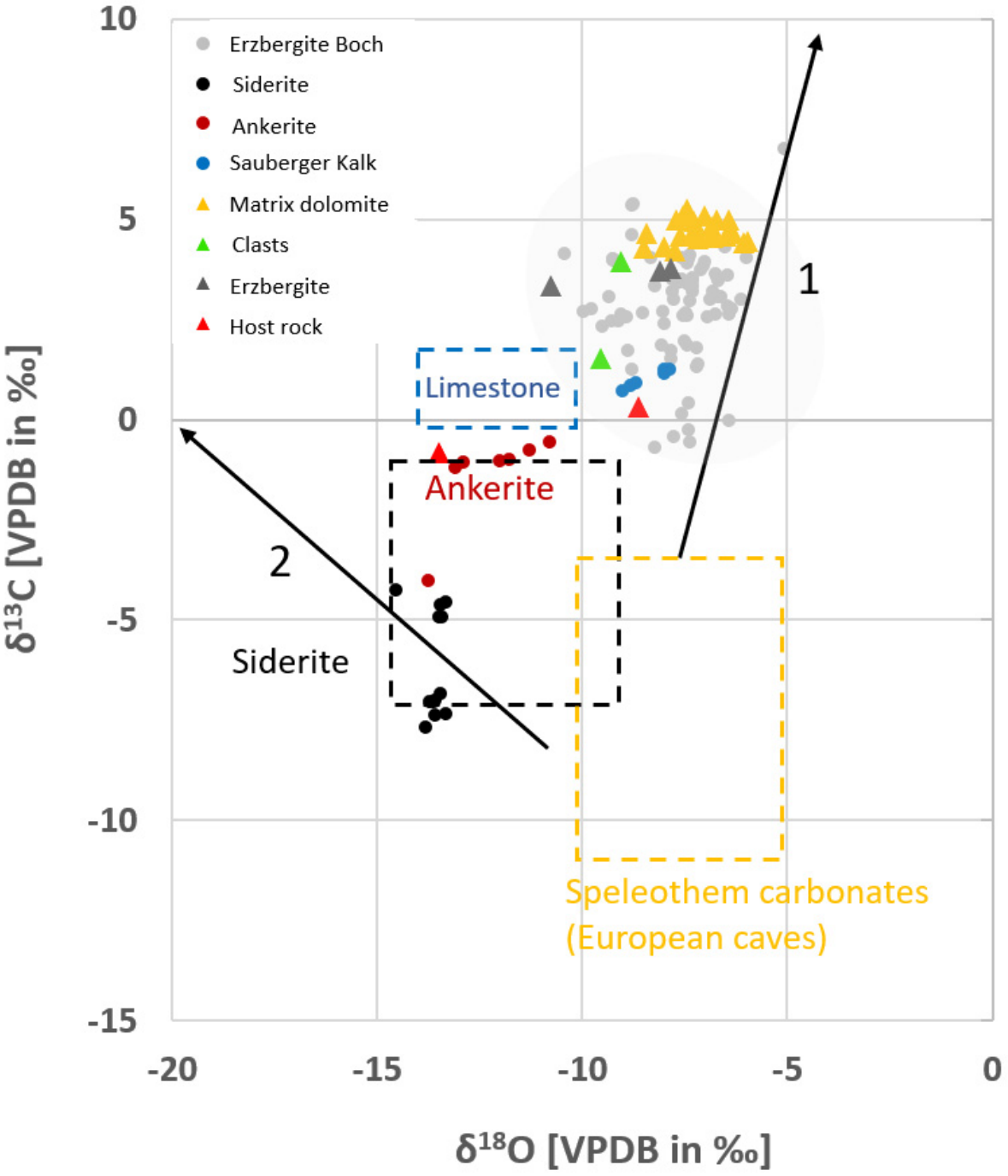

***Fig. 11**: Stable O versus C isotopic compositions of erzbergite (aragonite–calcite) precipitates, matrix dolomite (correlates to carbonate cataclasites) as well as of local host rock carbonates (siderite, ankerite, "Sauberger Kalk"). Triangles represent new data from this study whereas circles mark results from Boch et al. (2019). The dotted rectangles show isotope ranges for siderite/ankerite (black) and limestone (blue) reported in Weber (1997). Note the major differences between the different host rock carbonates. Additionally, the yellow field represents measured C and O isotope signatures of speleothem carbonates from different European caves (Žák et al., 2008). Two trends can be described in speleothem environments: Path 1 evolution of fine-grained CCC powders, controlled by kinetic isotope fractionation caused by fast water freezing and Path 2) evolution of coarse-grained CCC types formed during slow water freezing (Žák et al., 2008). All Ca-Mg carbonate vein mineralizations at the Erzberg follow the reaction path 1.*

4.6 Hydrogeochemical modelling

SI values of the most important Ca-Mg carbonates and of the Fe-oxyhdyroxides with respect to modern waters collected from different sections at the Erzberg are reported in Table 6. Results show that aragonite, calcite and dolomite as well as goethite and hematite are strongly supersaturated. The cross-plot of the SI of dolomite against the Mg:Ca molar ratio of Erzberg waters indicates that the southern section bears the highest potential for dolomite precipitation, which is consistent with the field observations (Fig. 12).

Table 6: *Mean SI values of different Ca-Mg carbonates and Fe-oxyhydroxides across the Erzberg waters. The Mg:Ca molar ratio refers to water composition at different sections at the Erzberg.*

SI values	Dolomite	Aragonite	Calcite	Goethite	Hematite	Mg:Ca
North	1.95	0.74	0.89	6.79	15.54	1.6
Central	2.60	1.03	1.18	6.88	15.71	2.4
South	3.08	0.74	0.88	6.29	14.56	17.8

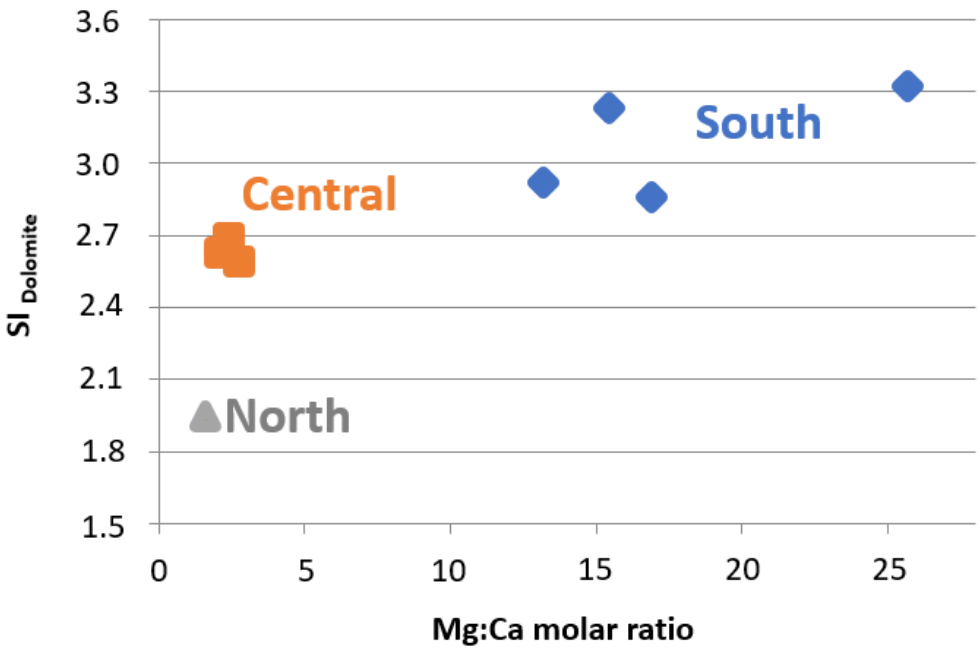

Fig. 12*: Cross-plot of the Mg:Ca molar ratio versus* $SI_{Dolomite}$ *showing the highest dolomitization potential at the southern section at the Erzberg.*

5. DISCUSSION

5.1. Distinction of Erzberg dolomite from modern marine analogues

Modern sedimentary dolomite typically possesses an excess of Ca versus Mg concentrations. Resulting from the non-stoichiometric composition and poorly ordered structure, modern Ca-Mg carbonate deposits are often referred to as proto-dolomite (Warren, 2000). Once the proto-dolomite is formed (very frequent with the aid of microbial mediation), subsequent transformation and aging processes, like recrystallization during Ostwald-ripening connected with burial diagenesis, yield more stoichiometric and ordered dolomite. These dolomites exhibit a higher stability (e.g. lower solubility) than the metastable proto-dolomite or its precursor phase(s) (Warren, 2000; Burns et al., 2000; Baldermann et al., 2015).

The Erzberg dolomites occur within a fundamentally different environment (e.g. continental-meteoric setting, fissured aquifer, very low temperature) compared to common marine dolomites (e.g. marine-evaporitic setting, microbial mediation, reducing conditions). Accordingly, they show unique petrographic (e.g. spheroidal to rhombohedral shapes, overgrowth features, replacement textures, zonation patterns) and geochemical (e.g. low Na, Sr, Fe and Mn contents, light O and heavy C isotopic compositions) signatures not reported for most of the modern marine analogues (Reinhold, 1998; Warren, 2000). Most importantly, the authigenic dolomites from the Erzberg have formed at very low temperatures (e.g. ~3 to 20 °C), and under oxic conditions. The characteristics of the Ca-Mg carbonate vein mineralizations at the Erzberg, particularly of the authigenic fracture dolomites, call for special paleo-environmental conditions at the onset and during carbonate mineral formation, which are discussed in the following.

5.2 Fracture formation and Neotectonic at the Erzberg

The most important prerequisite of forming the authigenic dolomite and erzbergite deposits at the Erzberg is the availability of open fissures and/or vertical fractures, which provide pathways for meteoric water infiltration as well as accommodation space for the carbonate sinter. Existing fault structures and possible reactivation of these faults or emergence of new fault systems in geologically young times at the Erzberg enable the formation of the prominent Ca-Mg carbonate vein infillings. U-Th age determinations of erzbergite samples collected at several locations across the Erzberg yield depositional ages from 285.1 ± 3.9 kyr BP to 1.03 ± 0.04 kyr BP (Boch et al., 2019). All erzbergite vein infillings recovered and analyzed from the southern section at the Erzberg show depositional ages younger than 19.21 to 18.86 kyr BP, with the youngest mineralizations being deposited from about 13.97 kyr BP onwards. Boch et al. (2019) have argued that the vertical fractures at the Erzberg are unlikely to have stayed open for a very long time, meaning that the first erzbergite generations precipitated immediately after fracture opening (e.g. the age of the erzbergites denotes the age of the fractures close after opening). Remarkably, all depositional ages of erzbergite deposits taken from the southern section fall around the Last Glacial Maximum or are younger, which supports the evidence for Neotectonic activity at the Erzberg.

5.3. Meteoric water infiltration

The hydrogeological system at the Erzberg can be described as a vadose fissured aquifer that intersects the Erzberg. Water flow paths are provided by existing (open) vertical faults and fractures cross-cutting the Erzberg. Ancient water flow routes are probably indicated by erzbergite (and dolomite) vein mineralizations clogging former open fractures. The residence time of the fracture and surface waters is considered to be relatively short (e.g. in the range of months to a few years), if considering the (i) geometry of the fractures, (ii) the expected high permeability of connected, fissured aquifers and (iii) the segregated drainage systems at the Erzberg (northern and central versus southern sections).

Boch et al. (2019) have divided the Erzberg into three sections (north, central and south) with respect to modern hydrogeochemistry (cf. Fig. 1) and concluded that most of the discovered erzbergite deposits and particularly the dolomitized intervals appear in the southern section of the Erzberg. In more detail, the water types differ from Mg-Ca-HCO_3 (north) and Mg-Ca-HCO_3-SO_4 (central) to Mg-HCO_3 (south) (cf. Table 1), with the southern water compositions being most beneficial for ongoing carbonate sinter formation, in line with field observations. The origin of these fluids has been recently clarified by Boch et al. (2019), e.g. based on δ^2H and $\delta^{18}O$ isotopic compositions: all surface and fracture water is of meteoric origin, plotting close to the

Local Austrian Meteoric Water Line (L-AMWL). Accordingly, the $\delta^{18}O$ values of the erzbergite samples are relatively low (-11.5 to -5.1 ‰, VPDB), corroborating the meteoric origin of the mineralizing fluids at the Erzberg.

5.4. Host rock dissolution

Compared to dissolution processes in karst regions in Austria and worldwide, where carbonic acid attack is responsible for carbonate mineral dissolution in the unsaturated (vadose) zone, a completely different dissolution process was observed at the Erzberg: generation of sulphuric acid due to weathering of iron sulphides (e.g., pyrite - an accessory phase in the Sauberger Kalk and in the mineralized sections) through reaction with oxidizing meteoric waters is considered to be the dominant hydrochemical mechanism causing host rock dissolution (Boch et al., 2019), as is expressed by equation 4:

$$2FeS_{2\,[s]} + 7.5O_2 + 7H_2O \rightarrow 2Fe(OH)_{3\,[s]} + 8H^+ + 4SO_4^{2-} \qquad (4)$$

High sulphate concentrations, ionic strength of the modern fracture waters and the obtained radiogenic Sr isotopic (cf. Appendix) composition of the host rocks, authigenic Erzberg carbonates and modern waters may support this conceptual reaction sequence. Dissolution of different host rocks (e.g., “Sauberger Kalk" and iron ore carbonates) is likely to mobilize various elements and components (like Ca, Mg, Fe and HCO_3^-), which can then be enriched along the water flow paths. A large contribution of soil derived carbonic acid attack to host rock dissolution can be excluded, because such a process would affect the $\delta^{13}C$ values (e.g. shift to lighter isotopic signatures of the precipitated carbonates, which is not seen). Boch et al. (2019) have expressed the dissolution of various host rock carbonates via sulphuric acid attack with the following reaction (5):

$$(Ca_x, Fe_y, Mg_z)(CO_3)_{2[s]} + 4H^+ + 2SO_4^{2-} \rightarrow x \cdot Ca^{2+} + y \cdot Fe^{2+} + z \cdot Mg^{2+} + 2SO_4^{2-} + 2H_2O + 2CO_{2[g]} \qquad (5)$$

$$[x + y + z = 2]$$

5.5. Initial calcium carbonate precipitation

Enrichment of chemical elements (Ca and Mg in particular) along the water flow path as well as CO_2 degassing in the fissured aquifer, as it can be inferred from low P_{CO2} values and comparably heavy C isotopic compositions of the carbonate vein mineralizations and fracture waters, likely promoted the early formation of calcium carbonates under alkaline conditions. Indeed, CO_2 loss by outgassing explains the relatively high $\delta^{13}C$ values of the erzbergite samples (3.61 ± 0.20 ‰, VPDB) and of the two types of authigenic dolomite (4.72 ± 0.29 ‰, VPDB). In addition, also modern Erzberg waters yield high $\delta^{13}C$ values (2.4 to 3.8 ‰, VPDB), which suggests that these processes probably occur until recent, and matches with the calculated log P_{CO2} of -3.2 to -3.0. At several places at the Erzberg, aragonite precipitation was initiated once high Mg and Ca concentrations in the fluid and alkaline pH conditions have been established. In the southern section at the Erzberg, this situation was reached from about 19 kyr BP onwards, where the first erzbergite deposits have been observed and have formed following equation 6:

$$Ca^{2+}_{[aq]} + 2HCO^{-}_{3\,[aq]} \rightarrow CaCO_{3\,[s]} + H_2O + CO_2 \qquad (6)$$

Warren (2000) has mentioned that calcite formation is kinetically inhibited at high Mg concentrations in solution (e.g. the active growth sites of calcite nuclei are blocked by hydrated Mg ions) and that aragonite is the preferred $CaCO_3$ polymorph that forms at high Mg:Ca molar ratios. So far, aragonite does not incorporate Mg in significant amounts because Mg does not fit into the orthorhombic structure of aragonite. However, the Mg^{2+} - ion can be incorporated into the trigonal structure of calcite. As a result of the ongoing removal of Ca from the solution, induced by initial aragonite precipitation, the molar Mg:Ca ratio was progressively increasing along the water flow path, reaching very high molar Mg:Ca ratios of 13-26 in modern waters from the southern section at the Erzberg.

5.6. Fluid development and dolomitization events

Calculated saturation indices (SI values) indicate that the modern Erzberg waters are highly supersaturated with respect to aragonite, calcite as well as dolomite (Table 7). Dolomite SI-values exhibit maximum values in the southern section, where the cataclastic carbonates containing dolomite have been found. Certainly, several kinetic energy barriers (e.g., dehydration of Mg ions and energy required for crystal lattice ordering) hindering dolomite to

precipitate from supersaturated solution need to be overcome, especially at low temperature and in the absence of microbial activity. However, other studies have shown that very high Mg:Ca molar ratios (> ~7-8) enable the precipitation of authigenic dolomite via reactive intermediates (e.g. HMC).

$$Mg^{2+}_{[aq]} + Ca^{2+}_{[aq]} + 2HCO^{-}_{3\,[aq]} \rightarrow CaMg(CO_3)_{2\,[s]} + 2H_2O + 2CO_2 \qquad (7)$$

In the southern section at the Erzberg the reported high Mg:Ca ratio is driven by initial aragonite precipitation that causes an enrichment of Mg in the solution relative to Ca, subsequently triggering dolomite formation (equation 7) at two different events:

(i) A first dolomitization event, which induced the formation of the older spheroidal dolomite, occurred at approximately 19.2 to 18.8 kyr BP at 2.8 – 4.1 °C, i.e. at near freezing temperatures. This type of dolomite is characterized by a degree of cation ordering of 0.35 and large crystal size (> 100 μm) and builds up about ~5 vol% of the total dolomitized rock volume. Zonation patterns, seen in the BSE images (cf. Fig. 10 A, B), e.g., Ca-rich cores and Mg-rich rims, support the evidence for the development of a Ca-rich to a Mg-rich fluid during dolomite growth. The low concentration of redox-sensitive elements (Fe, Mn) in dolomite points to oxic conditions throughout dolomite nucleation and growth. The spheroidal texture of this dolomite type suggests the water flow rates were very low at the Erzberg at around the Last Glacial Maximum, where the first dolomite generation was formed. It seems that residual fluids could be the origin for these spheroidal dolomites, because they would enable long reaction times and ongoing rebound between precipitated (proto-) dolomite and the solution with further Mg exchange.

(ii) The second dolomitization event started at about 13.7-13.1 kyr BP and led to the deposition of the matrix dolomite. This dolomite type formed by replacement of former aragonite needles and represents ca. 95 vol.% of the total dolomite volume. Very small (~10 μm), planar s- to e-shape crystals and a lower cation ordering ratio of 0.25 are typical for this dolomite type. This matrix dolomite formed at warmer temperatures, compared to the spheroidal dolomite, in the range of 8.3 – 20.3 °C. Overgrowth structures of matrix dolomite on the older spheroidal dolomite and modern hydrogeochemistry at the Erzberg could indicate that matrix dolomite forms until recent. Higher temperatures may be associated with a higher flow rate and therefore less time for reactions between precipitates and fluids, explaining the lower Mg content and cation order in matrix dolomites.

5.7. Conceptual model of dolomite formation

From the present datasets, two different types of dolomite from the Erzberg can be distinguished: (i) “old and cold” spheroidal dolomite associated with fractures and (ii) “young and warm” matrix dolomite (sub-rounded to rhombohedral dolomite replacing aragonite matrix). These authigenic dolomites might have been formed in the following way (Fig. 13):

Stage 1 (before 19 kyr BP): Formation of fractures and faults during tectonic movements or gravitational events in the Pleistocene.

Stage 2 (before 19 kyr BP): Deposition of cataclasites in young fractures with clasts from worked up material from adjacent carbonate rocks (Sauberger Kalk and iron ore carbonates).

Stage 3 (before 19 kyr BP): Meteoric water infiltration and development of a fissured aquifer, where sulphuric acid is generated (due to the oxidation of accessory sulphides), causing dissolution of host rock carbonates and development of mineralized fluid rich in Ca^{2+}, Mg^{2+} and HCO_3^- ions.

Stage 4 (~ 19 kyr BP): Initial precipitation of aragonite in fractures through degassing of CO_2 causes an enrichment of Mg relative to Ca in the residual fluid.

Stage 5 (19 -14 kyr BP): First dolomitization event: deposition of spheroidal dolomite in fissures and cracks. Subsequent changes in the hydrological system (transition from vadose to phreatic water flow)

Stage 6 (14 kyr BP until recent): Second dolomitization event: formation of matrix dolomite and development of new aragonite-calcite vein systems and sub-recent dolomitization.

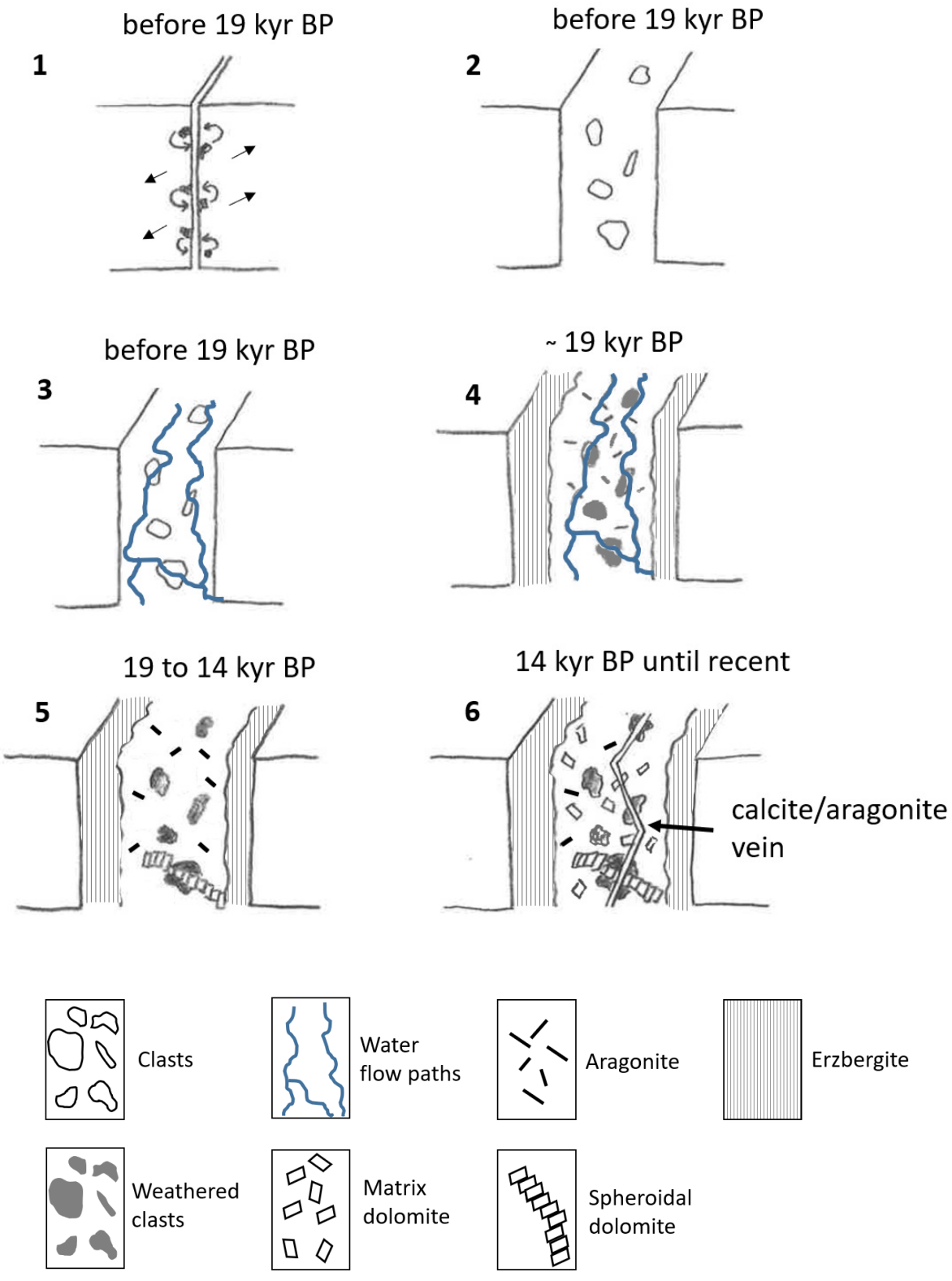

Fig. 13: *Schematic model showing the formation of Ca-Mg carbonate vein infillings in young vertical fractures at the Erzberg. See text for detailed explanations.*

5.8. Broader implications of dolomite formation at near-freezing temperatures

Continental dolomites have the potential to be used as a paleo-climatic and paleo-environmental archive. They can be used for reconstructing carbonate depositional ages, paleo-temperatures as well as for backtracking former hydrogeological systems, including the analyses of water sources and ancient water flow paths. Also, the weathering regime and past fluid-rock interaction mechanisms can be determined from these vein mineralizations, e.g. by using O, C and radiogenic Sr isotopes. Different crystallization styles and paleo-redox conditions can be reconstructed from dolomite textures and trace element contents.

The precipitation process of the continental dolomites at the Erzberg, as it can be inferred from the present datasets, is a novelty in modern dolomite research, as most factors recently and historically considered to induce dolomite precipitation are not active, e.g. high temperatures and microbial mediation. Indeed, the fracture dolomites at the Erzberg started forming at near-freezing temperatures, following a highly complex evolutionary history of the mineralizing meteoric solutions and initial erzbergite precipitates. Such conditions may have also prevailed in various other high-altitude mountainous regions worldwide; yet detailed petrographic studies are lacking that confirm the presence of authigenic fracture dolomites in such settings. Future studies should also explore the existence of sedimentary dolomites in other low temperature environments, such as in permafrost regions as well as in ice caves, and their potential use as an environmental archive. For example, modern dolomite formation processes could be studied by investigation of permafrost soils in Siberia, where cyclic water-freezing processes lead to an extreme enrichment of Mg over Ca in the residual fluids from which dolomite (or its reactive intermediates) is likely to precipitate.

Moreover, studying continental carbonate archives has the great potential to extend knowledge and all types of accumulated datasets (climatic, environmental, etc.) established from the investigation of marine carbonate-depositing settings. Noteworthy, continental carbonates and/or fracture dolomites are mostly formed without (extended) influence of microorganisms, in contrast to all marine carbonates known so far. Metabolism of carbonate-producing organisms often results in huge elemental and isotopic shifts in the carbonates (known as vital effects), which can smear the ambient environmental conditions prevailing during carbonate mineral deposition. In this context, continental carbonates, if not subjected to alteration, should record the primary formation conditions without biological irradiation. In essence, continental-meteoric fracture-bound dolomites and carbonates formed at low temperature should be considered as a new paleo-environmental archive; yet their occurrence in other cold setting (permafrost regions) has to be confirmed and their applicability in paleo-climate research assessed.

6. SUMMARY AND CONCLUSION

The investigation of carbonate vein deposits in the southern section at the Erzberg (Styria, Austria) yielded the following key findings:

1. Three different vein infillings were observed: (i) A dark brown carbonate layer, (ii) a bright beige carbonate layer and (iii) laminated erzbergite, which was found on both sites as well as between the carbonate layers. U-Th age dating of these erzbergites resulted in ages about 19.21 kyr BP to 13.11 kyr BP, suggesting a very young age of the fractures itself and their carbonate vein deposits.

2. Petrographic, mineralogical and electron microscope observations of both carbonate layers confirmed the existence of two different generations of continental (low temperature) dolomite: (i) A near-stoichiometric spheroidal dolomite (~ 51 mol% $CaCO_3$) with a moderate COD (0.35) and zonation patterns with Ca-rich cores and Mg-rich rims. This type precipitated at about 19 kyr BP at formation temperatures between 2.8 to 4.1 °C. (ii) A matrix-replaced, Ca-excess dolomite (~54 mol% $CaCO_3$) with a low COD (0.25), that represents 95 % of the dolomite volume in the carbonate cataclastic layers. The younger matrix dolomite (14 kyr BP) originated at temperatures ranging between 8.3 to 20.3 °C. The overall low formation temperatures are also reflected in low $\delta^{18}O$ signatures of the dolomites that reveal average values of about -7.2 ± 0.7 ‰ VPDB.

3. Dissolution of different host rocks as (i) Devonian limestone the so-called “Sauberger Kalk” and (ii) iron ores carbonates (confirmed by Sr-isotope measurements) are the reason for the high Mg, Ca and HCO_3^- concentration in the solution. CO_2 degassing (traced by heavy $\delta^{13}C$ signatures) favoured the precipitation process of aragonite that in turn causes very high aqueous Mg:Ca molar ratios of 14 to 26 and a high saturation index for dolomite ($SI_{Dolomite}$ = 3.08). Ongoing CO_2 degassing subsequently enabled dolomite formation.

4. A schematic model was developed to display the evolution of the authigenic continental low temperature dolomites: Sulphuric acid evolution and meteoric water inflow in open fractures at the Erzberg are the reasons for host rock dissolution. Initial aragonite precipitation caused an enrichment of the Mg:Ca molar ratio in the solution. Two dolomitization events occurred, in which authigenic dolomite was formed (i) by direct precipitation from residual fluids and/or (ii) replacement of $CaCO_3$ precursor phases, perhaps following the sequence aragonite → low-Mg calcite → high-Mg calcite → disordered dolomite → more ordered dolomite.

5. Investigations and paleo-environmental studies focusing on continental authigenic dolomites build an innovation in dolomite research and may lead to new conclusions and insights concerning enigmatic dolomite formations in exotic (low temperature) environments.

7. REFERENCES

Alonso-Zarza A. M. and Martín-Pérez A. (2008) Dolomite in caves: Recent dolomite formation in oxic, non-sulfate environments. Castañar Cave, Spain. *Sedimentary Geology* **205**, 160–164.

Angel F. (1939) Unser Erzberg. *Naturwissenschaftlicher Verein für Steiermark* **75**, 227–321.

Baldermann A., Deditius A. P., Dietzel M., Fichtner V., Fischer C., Hippler D., Leis A., Baldermann C., Mavromatis V., Stickler C. P. and Strauss H. (2015) The role of bacterial sulfate reduction during dolomite precipitation: Implications from Upper Jurassic platform carbonates. *Chemical Geology* **412**, 1–14.

Belocky R. (1992) Regional vergleichende Untersuchung lagerstättenbildender Fluide in den Ostalpen als Hinweis auf eine mögliche metamorphe Ableitung. *PhD Thesis Univ. Braunschweig*, 1–103.

Beran A. and Thalmann F. (1977) Feinkörnige gebänderte Siderite im Spateisensteinbergbau Radmer-Buchegg. *Österr. Akad. Wiss.* **Math.-Naturwiss. Kl., 4**, 57–62.

Boch R., Wang X., Kluge T., Leis A., Lin K., Pluch H., Mittermayr F., Baldermann A., Böttcher M. E. and Dietzel M. (2019) Aragonite-calcite veins of the 'Erzberg' iron ore deposit (Austria): Environmental implications from young fractures. *Sedimentology* **66**, 604–635.

Bontognali T. R. R., McKenzie J. A., Warthmann R. J. and Vasconcelos C. (2014) Microbially influenced formation of Mg-calcite and Ca-dolomite in the presence of exopolymeric substances produced by sulphate-reducing bacteria. *Terra Nova* **26**, 72–77.

Bontognali T. R. R., Vasconcelos C., Warthmann R. J., Bernasconi S. M., Dupraz C., Strohmenger C. J. and McKenzie J. A. (2010) Dolomite formation within microbial mats in the coastal sabkha of Abu Dhabi (United Arab Emirates). *Sedimentology* **57**, 824–844.

Burns S. J., McKenzie J. A. and Vasconcelos C. (2000) Dolomite formation and biogeochemical cycles in the Phanerozoic. *Sedimentology* **47**, 49–61.

De Boever E., Brasier A. T., Foubert A. and Kele S. (2017) What do we really know about early diagenesis of non-marine carbonates? *Sedimentary Geology* **361**, 25–51.

Deng S., Dong H., Lv G., Jiang H., Yu B. and Bishop M. E. (2010) Microbial dolomite precipitation using sulfate reducing and halophilic bacteria: results from Qinghai Lake, Tibetan Plateau, NW China. *Chemical Geology* **278**, 151–159.

Dupraz C., Reid R. P., Braissant O., Decho A. W., Norman R. S. and Visscher P. T. (2009) Processes of carbonate precipitation in modern microbial mats. *Earth-Science Reviews* **96**, 141–162.

Flügel E. (2004) Microfacies of carbonate rocks: Analysis, interpretation and application. *Springer-Verlag, Berlin, Heidelberg, New York* (976 pp.).

Füchtbauer H. and Goldschmidt H. (1965) Beziehungen zwischen Calciumgehalt und Bildungsbedingungen der Dolomite. *Geologische Rundschau* **55**, 29–40.

Füchtbauer H. and Richter D. K. (1988) Karbonatgesteine. In *Füchtbauer H (Hrsg.) Sedimente und Sedimentgesteine. E. Schweizerbart'sche Verlagsbuchhandlung, Stuttgart, 1141 S*.

Galy A., Belshaw N. S., Halicz L. and O'Nions R.K. (2001) High-precision measurement of magnesium isotopes by multiple-collector inductively coupled plasma mass spectrometry. *International Journal of Mass Spectrometry* **208**, 89–98.

Galy A., Yoffe O., Janney P. E., Williams R. W., Cloquet C., Alard O., Halicz L., Wadhwa M., Hutcheon I. D., Ramon E. and Carignan J. (2003) Magnesium isotope heterogeneity of the isotopic standard SRM980 and new reference materials for magnesium-isotope-ratio measurements. *J. Anal. At. Spectrom.* **18**, 1352–1356.

Geske A., Goldstein R. H., Mavromatis V., Richter D. K., Buhl D., Kluge T., John C. M. and Immenhauser A. (2015) The magnesium isotope (δ26Mg) signature of dolomites. *Geochimica et Cosmochimica Acta* **149**, 131–151.

Hardy R. G. and Tucker M. (1988) X-ray powder diffraction of sediments. In *Techniques in sedimentology* (ed. M. Tucker). Blackwell Scientific Publications.

Hatle E. (1892) Fünfter Beitrag zur mineralogischen Topographie der Steiermark. *Mitt. Naturw. Ver. Steiermark* **28**, 294 - 308.

Irion G. and Müller G. (1968) Huntite, Dolomite, Magnesite and Polyhalite of Recent Age from Tuz Gölü, Turkey. *Nature* **220**, 1309–1310.

Land L. S. (1980) The isotopic and trace element geochemistry of dolomite: The state of the art. In *Concepts and Models of Dolomitization* (eds. D. H. Zenger, J. B. Dunham and R. L. Ethington). SEPM (Society for Sedimentary Geology), pp. 87–110.

Land L. S. (1998) Failure to precipitate dolomite at 25°C from dilute solution despite 1000-fold oversaturation after 32 years. *Aquatic Geochemistry* **4**, 361–368.

Lippmann F. (1973) Sedimentary Carbonate Minerals. *Springer-Verlag*, Berlin (228 pp.).

Lumsden D. N. and Chimahusky J. S. (1980) Relationship between dolomite nonstoichiometry and carbonate facies parameters. In *Concepts and Models of Dolomitization* (eds. D. H. Zenger, J. B. Dunham and R. L. Ethington). SEPM (Society for Sedimentary Geology), pp. 123–137.

Meister P., Reyes C., Beaumont W., Rincon M., Collins L., Berelson W., Stott L., Corsetti F. and Nealson K. H. (2011) Calcium and magnesium-limited dolomite precipitation at Deep Springs Lake, California. *Sedimentology* **58**, 1810–1830.

Meixner H. (1970) Anschliffbeobachtungen zu verschiedenen Metasomatosen in österreichischen Lagerstätten karbonatischer Eisenerze. *Archiv für Lagerstätten in den Ostalpen* **10**, 61–74.

Middelburg J. J., Lange G. J. d. and Kreulen R. (1990) Dolomite formation in anoxic sediments of Kau Bay, Indonesia. *Geology* **18**, 399.

Moore C. H. and Wade W. J. (2013) *Carbonate reservoirs. Porosity and diagenesis in a sequence stratigraphic framework.* 2nd ed. Elsevier, Amsterdam (392 pp.).

Müller G. (1970) High-magnesian calcite and protodolomite in Lake Balaton (Hungary) sediments. *Nature* **226**, 749–750.

Müller G., Irion G. and Förstner U. (1972) Formation and diagenesis of inorganic Ca-Mg carbonates in the lacustrine environment. *Naturwissenschaften* **59**, 158–164.

Parkhurst D. and Appelo T. (2013) Description of input and examples for PHREEQC version 3—a computer program for speciation, batch-reaction, one-dimensional transport, and inverse geochemical calculations. *US Geological Survey Techniques and Methods* book 6, chap A43, 497.

Prochaska W. (1997) Formation of different siderite provinces during the Alpine tectono-metamorphic event in the Eastern Alps of Austria-In: *Mineral Deposits Research and Exploration*, 845–848.

Prochaska W. (2012) Siderite and magnesite mineralizations in Palaeozoic strata of the Eastern Alps (Austria). *Journal of Alpine Geology*, 309–322.

Prochaska W. (2016) Genetic concepts on the formation of the Austrian magnesite and siderite mineralizations in the Eastern Alps of Austria. *Geol Cro* **69**, 31–38.

Reinhold C. (1998) Multiple episodes of dolomitization and dolomite recrystallization during shallow burial in Upper Jurassic shelf carbonates: eastern Swabian Alb, southern Germany. *Sedimentary Geology* **121**, 71–95.

Richter D. K., Meissner P., Immenhauser A., Schulte U. and Dorsten I. (2010) Cryogenic and non-cryogenic pool calcites indicating permafrost and non-permafrost periods: a case study from the Herbstlabyrinth-Advent Cave system (Germany). *The Cryosphere* **4**, 501–509.

Royce C. F., Wadell J. S. and Petersen L. E. (1971) X-Ray Determination of Calcite-Dolomite: an Evaluation. *SEPM Journal of Sedimentary Research* **Vol. 41**, 483–488.

Sánchez-Román M., McKenzie J. A., Luca Rebello Wagener A. de, Rivadeneyra M. A. and Vasconcelos C. (2009) Presence of sulfate does not inhibit low-temperature dolomite precipitation. *Earth and Planetary Science Letters* **285**, 131–139.

Schönlaub H. P., Flajs G. and Thalmann F. (1980) Conodontenstratigraphie am Steirischen Erzberg (Nördliche Grauwackenzone). *Jahrb. Geol. B.-A.* **123**, 169–229.

Schönlaub H.-P. (1982) Die Grauwackenzone in den Eisenerzer Alpen (Österreich). *Jahrb. Geol. B.-A.* **124**, 361–423.

Schouppe A. v. (1854) Geognostische Bemerkungen über den Erzberg bei Eisenerz. *Jahrbuch d. Geologischen Reichsanstalt* **5**, 396–405.

Schulz O., Vavtar F. and Dieber K. (1997) Die Siderit-Erzlagerstätte Steirischer Erzberg: Eine geowissenschaftliche Studie, mit wirtschaftlicher und geschichtlicher Betrachtung. *Arch. Lagerst. forsch. Geol. B.-A.* **20**, 65–178.

Sibley D. F. and Gregg J. M. (1987) Classification of Dolomite Rock Textures. *Journal of Sedimentary Petrology* **57**, 967–975.

Spindler P. (1992) Neue Untersuchungen zur Mineralogie und Geochemie der Basisbreccie des Steirischen Erzberges, Österreich. *Österr. Akad. Wiss.*, math.- naturwiss. Kl., 1–25.

Swart P. K. (2015) The geochemistry of carbonate diagenesis: The past, present and future. *Sedimentology* **62**, 1233–1304.

Tucker M. E. and Wright V. P. (1990) Carbonate sedimentology. *Blackwell Scientific Publications, Oxford.*

Vacek M. (1900) Skizze eines geologischen Profiles durch den steirischen Erzberg. *Jahrb. d. k. k. Geolog. Reichsanstalt* **50**.

Vasconcelos C. and McKenzie J. A. (1997) Microbial mediation of modern dolomite precipitation and diagenesis under anoxic conditions (Lagoa Vermelha, Rio de Janeiro, Brazil). *Journal of Sedimentary Research* **Vol. 67**, 378–390.

Vasconcelos C., McKenzie J. A., Bernasconi S., Grujic D. and Tiens A. J. (1995) Microbial mediation as a possible mechanism for natural dolomite formation at low temperatures. *Nature* **377**, 220–222.

Veetil S. P., Mucci A. and Arakaki T. (2018) Dolomite dissolution kinetics in aqueous solutions in the presence of organic and inorganic additives at 25 °C and pCO2 ~ 1 atm. *Chemical Geology* **483**, 98–110.

Wacey D., Wright D. T. and Boyce A. J. (2007) A stable isotope study of microbial dolomite formation in the Coorong Region, South Australia. *Chemical Geology* **244**, 155–174.

Warren J. (2000) Dolomite: occurrence, evolution and economically important associations. *Earth-Science Reviews* **52**, 1–81.

Warthmann R., Vasconcelos C., Sass H. and McKenzie J. A. (2005) Desulfovibrio brasiliensis sp. nov., a moderate halophilic sulfate-reducing bacterium from Lagoa Vermelha (Brazil) mediating dolomite formation. *Extremophiles : life under extreme conditions* **9**, 255–261.

Weber L. (1997) Metallogenetische Karte von Österreich (1: 500.000) und Handbuch der Lagerstätten der Erze, Industrieminerale und Energierohstoffe Österreichs. *Arch. Lagerst. forsch. Geol. B.-A.* **19**, 1–607.

Wombacher F., Eisenhauer A., Heuser A. and Weyer S. (2009) Separation of Mg, Ca and Fe from geological reference materials for stable isotope ratio analyses by MC-ICP-MS and double-spike TIMS. *J. Anal. At. Spectrom.* **24**, 627–636.

Žák K., Onac B. P., Kadebskaya O. I., Filippi M., Dublyansky Y. and Luetscher M. (2018) Cryogenic Mineral Formation in Caves. In *Ice Caves.* Elsevier, pp. 123–162.

Žák K., Onac B. P. and Perşoiu A. (2008) Cryogenic carbonates in cave environments: A review. *Quaternary International* **187**, 84–96.

Žák K., Urban J., Cílek V. and Hercman H. (2004) Cryogenic cave calcite from several Central European caves: age, carbon and oxygen isotopes and a genetic model. *Chemical Geology* **206**, 119–136.

8. TABLE OF FIGURES

9. LIST OF TABLES

10. APPENDIX

Raw data

XRD

Table S 1: Quantification of X-ray diffractogramms of all 13 bulk samples. The following mineral phases have been identified and are listed below in [wt%]: Ca-exess dolomite (Ca-excess Dol), dolomite (Dol), quartz (Qtz), goethite (Gth), hematite (Hem), calcite (Cal), muscovite (Ms) and aragonite (Arg)

Sample-ID	Ca-excess Dol	Dol	Qtz	Gth	Hem	Cal	Ms	Arg
1	0.0	0.0	0.0	0.0	0.0	1.7	0.0	98.3
2	62.7	12.4	5.0	6.6	3.9	1.9	6.2	1.2
3	66.9	11.1	4.5	5.7	4.5	1.8	4.1	1.3
4	59.2	8.6	4.8	7.5	9.8	4.2	2.2	3.8
5	18.8	2.5	1.4	0.3	0.1	3.3	0.7	72.9
6	23.3	0.5	2.5	0.1	0.7	2.9	1.0	68.9
7	54.4	15.5	3.5	2.9	0.5	6.6	4.1	12.5
8	63.1	17.0	4.5	3.6	0.3	4.0	3.6	3.9
9	65.6	16.2	5.5	2.0	0.2	3.3	4.0	3.2
10	60.5	14.8	4.7	5.4	0.9	3.6	6.7	3.4
11	62.8	15.6	4.4	6.2	0.6	3.7	3.9	2.8
12	74.3	11.8	5.0	1.6	0.6	1.6	3.4	1.8
13	0.0	0.0	0.0	0.0	0.0	0.8	0.0	99.2

Table S 2: Calculated mol% $CaCO_3$ by using the position of the $d_{(104)}$ peak.

Sample-ID	$d_{(104)}$	mol%$CaCO_3$
1	-	-
2	2.898	54.0
3	2.894	52.7
4	2.896	53.3
5	2.896	53.3
6	2.889	51.0
7	2.892	52.0
8	2.892	52.0
9	2.892	52.0
10	2.895	53.0
11	2.895	53.0
12	2.893	52.3
13	-	-
3_B_4	2.904	55.8
3_C_3	2.905	56.2
4_A_9	2.896	53.2
4_A_16	2.895	52.8

XRF

Table S 3: Calculated Oxides in wt% as well as the analyzed LOI of all bulk samples (1-13) and different comparison samples.

Probe	MgO	Al_2O_3	SiO_2	CaO	MnO	Fe_2O_3	Sr	P_2O_5	K_2O	TiO_2	Na_2O	LOI	Summe
1	0.08	0.27	0.54	55.28	0.03	0.44	0.01	0	0	0	0	43.35	100
2	12.76	2.32	7.71	21.84	0.96	20.4	0	0.06	0.47	0.09	0	33.39	100
3	12.49	2.1	7.11	21.22	0.97	19.72	0	2.4	0.46	0.1	0	33.44	100.01
4	11.24	2.08	6.83	22.29	1.12	23.5	0	0.05	0.33	0.1	0.09	32.37	100
5	2.72	0.76	1.98	49.41	0.18	2.93	0.01	0.01	0.07	0	0	41.89	99.96
6	3.7	1.15	3.52	47.13	0.16	2.73	0.01	0.02	0	0	0.12	41.45	99.99
7	13.43	2.59	7.1	30.23	0.4	6.63	0	0.06	0.49	0.09	0	38.95	99.97
8	15.52	2.53	8.17	27.05	0.4	6.93	0	0.07	0.57	0.08	0	38.66	99.98
9	14.99	2.76	8.8	27.4	0.34	6.2	0	0.07	0.66	0	0	38.75	99.97
10	14.03	2.73	8.54	26.24	0.49	9.99	0	0.09	0.63	0.12	0	37.13	99.99
11	14.12	2.91	8.24	25.87	0.47	10.66	0	0.1	0.5	0.1	0.09	36.95	100.01
12	15.78	2.52	7.52	26.89	0.38	6.72	0	0.1	0.44	0.1	0.1	39.43	99.98
13	0	0.02	0.12	56.15	0	0.04	0.01	0	0	0	0	43.67	100.01
1_C	0.3	13.9	77.99	0.51	0	0.86	0	0.09	3.2	0.17	0.2	2.75	99.97
3_C	14.52	2.2	7.09	24.24	0.73	14.4	0	0.05	0.48	0.08	0	36.2	99.99
4_B	14	2.97	8.8	27.21	0.44	7.74	0	0.1	0.74	0.12	0	37.88	100
5_B	13.92	3.15	7.88	20.86	0.8	18.34	0	0.1	0.45	0.1	0.11	34.29	100
6_A	1.89	5.3	17.22	5.56	2.29	49.89	0	0.09	1.34	0.3	0.25	15.88	100.01
6_B	0.86	2.43	16.53	6.95	2.93	56.94	0	0.07	0.53	0.09	0.18	12.42	99.93

ICP-OES

Table S 4: Complete ICP-OES results of all measured bulk samples (AZ-1 solid to AZ13- solid) as well as from comparison samples.

Analyte Name	Calib Units	AZ-1solid	AZ-2solid	AZ-3solid	AZ-4solid	AZ-5solid	AZ-6solid	AZ-7solid	AZ-8solid	AZ-9solid	AZ-10solid
Al	ug/L	567945	2732611	2958846	3586076	1219898	1971223	2693275	2692210	2548536	2196389
Ba	ug/L	1647	37353	40390	41017	6440	13462	27202	31714	24798	29921
Ca	mg/L	358947	141209	143146	145892	330423	312904	204665	184580	183271	180334
Co	ug/L	7176	5469	< 1000	2111	9481	< 1000	6291	17469	11497	7067
Cr	ug/L	< 1000	6468	15151	< 1000	< 1000	< 1000	10557	< 1000	18950	2944
Cu	ug/L	< 1000	< 1000	< 1000	< 1000	< 1000	< 1000	< 1000	< 1000	< 1000	< 1000
Fe	ug/L	2907319	106877071	109786220	126216073	20397793	18140920	43389037	45994308	39210709	60081566
K	mg/L	416	1178	1367	1496	645	992	1438	1538	1502	1471
Li	ug/L	< 1000	2859	2877	2829	1332	1711	2757	2764	2651	2469
Mg	mg/L	396	66806	68328	58784	14232	19680	70397	81646	82298	79576
Mn	ug/L	276066	4331987	4591889	4969757	1569629	1308974	2568816	2958288	2253947	3009344
Na	mg/L	< 10	< 10	< 10	< 10	< 10	< 10	38	45	31	41
Ni	ug/L	< 1000	23888	23659	30150	9390	8190	5296	7037	3447	< 1000
Si	mg/L	742	5699	6204	7240	1926	3008	4605	4793	4503	4523
Sr	ug/L	81888	14680	14376	20359	80750	77670	31827	20409	19608	21538
Zn	ug/L	< 1000	< 1000	< 1000	2654	2893	2966	2833	< 1000	< 1000	< 1000

Table S 5: Complete ICP-OES results of all measured bulk samples (AZ-1 solid to AZ13- solid) as well as from comparison samples.

Analyte Name	Calib Units	AZ-11solid	AZ-12solid	AZ-13solid	AZ-1Csolid	AZ-3Csolid	AZ-4Bsolid	AZ-5Bsolid	AZ-6Asolid	AZ-6Bsolid
Al	ug/L	2623174	2949596	138267	11476938	2280871	2665548	4293681	3720514	1579652
Ba	ug/L	28143	32286	< 1000	122594	26797	33538	45878	64524	50592
Ca	mg/L	174709	186580	366989	3747	161020	187252	141337	39491	47164
Co	ug/L	8070	8618	4482	< 1000	5238	9714	5201	< 1000	< 1000
Cr	ug/L	9871	10927	< 1000	< 1000	9244	17470	< 1000	< 1000	< 1000
Cu	ug/L	< 1000	< 1000	< 1000	< 1000	< 1000	< 1000	< 1000	< 1000	< 1000
Fe	ug/L	64647733	44882789	231191	3668493	84846805	49167881	107370034	284218741	222590735
K	mg/L	1566	1760	57	6475	1211	1465	1675	2787	1536
Li	ug/L	2558	2833	< 1000	2909	2888	2523	4449	1234	< 1000
Mg	mg/L	77653	89797	119	541	78433	77998	78505	9826	3663
Mn	ug/L	3198024	2649787	19526	220787	4133726	3184177	4665297	16727501	6670783
Na	mg/L	< 10	< 10	14	172	< 10	18	115	< 10	< 10
Ni	ug/L	29269	4907	< 1000	6026	8215	19950	15187	5234	31085
Si	mg/L	5063	5370	152	16897	4909	4897	7674	8831	6769
Sr	ug/L	20369	17664	73544	3728	14407	19993	12691	12834	20042
Zn	ug/L	< 1000	1514	< 1000	< 1000	< 1000	< 1000	2663	9151	< 1000

C- and O-isotopes

Table S 6: $\delta^{13}C$ and $\delta^{18}O$ [in ‰, VPDB] results from dolomite containing carbonate cataclasite (Dol), erzbergite (EB), host rock and clasts.

Sample ID	Rock type	Description	$\delta^{13}C$ [VPDB] in [‰]	$\delta^{18}O$ [VPDB] in [‰]
3_C_1	Dol	Matrix dolomite (type 2)	4.60	-7.62
3_C_2	Dol	Matrix dolomite (type 2)	4.65	-8.44
3_C_3	Dol	Matrix dolomite (type 2)	5.27	-7.44
3_B_4	Dol	Matrix dolomite (type 2)	4.98	-7.70
3_B_5	Dol	Matrix dolomite (type 2)	4.82	-6.87
3_D_6	Dol	Matrix dolomite (type 2)	4.54	-6.84
3_D_7	Dol	Matrix dolomite (type 2)	4.72	-7.23
4_A_8	Dol	Matrix dolomite (type 1)	4.53	-7.20
4_A_9	Dol	Matrix dolomite (type 1)	4.65	-6.33
4_A_10	Dol	Matrix dolomite (type 1)	5.00	-6.42
4_A_11	Dol	Matrix dolomite (type 2)	5.00	-6.72
4_A_12	Dol	Matrix dolomite (type 2)	4.22	-7.74
4_A_13	Dol	Matrix dolomite (type 2)	4.66	-7.32
4_A_14	Dol	Matrix dolomite (type 2)	4.30	-8.02
4_A_15	Dol	Matrix dolomite (type 2)	4.28	-8.51
4_A_16	Dol	Matrix dolomite (type 2)	4.61	-6.81
4_A_17	Dol	Matrix dolomite (type 1)	4.46	-5.98
4_A_18	Dol	Matrix dolomite (type 1)	4.43	-6.08
4_A_19	Dol	Matrix dolomite (type 1)	4.57	-6.50
5_A_20	Dol	Matrix dolomite (type 2)	5.10	-7.03
5_A_21	Dol	Matrix dolomite (type 2)	5.14	-7.42
5_A_22	Dol	Matrix dolomite (type 2)	5.10	-7.54
5_A_23	Dol	Matrix dolomite (type 2)	4.94	-7.28
4_A_24	Clast	Fe-Oxyhydroxide	1.54	-9.54
4_A_25	Clast	Fe-Oxyhydroxide	3.96	-9.05
4_A_26	EB	Aragonite (Calcite)	3.79	-7.84
4_A_27	EB	Aragonite (Calcite)	3.70	-8.09
4_A_28	EB	Aragonite (Calcite)	3.33	-10.78
6_A_29	Host rock	Ore (Ankerite)	0.31	-8.63
6_A_30	Host rock	Ore (Ankerite)	-0.82	-13.50

Mg-isotopes

The $\delta^{26}Mg$ isotopic compositions of the investigated carbonate cataclasites type 1 and type 2 range between -1.73 ‰ to -2.33 ‰ with a mean $\delta^{26}Mg$ value of -1.98 ± 0.49 ‰ (2σ, n = 4). The $\delta^{26}Mg$ composition of recent water samples ranges from -1.01 ‰ to -1.29 ‰, resulting in a mean $\delta^{26}Mg$ value of -1.15 ± 0.28 ‰ (2σ, n = 2). A summary of the obtained $\delta^{26}Mg$ (and $\delta^{25}Mg$) isotopic compositions is provided in Table S 7.

Table S 7: : $\delta^{25}Mg$ and $\delta^{26}Mg$ isotope values and 2σ for three Mg standards (DSM3, CAM1, JDO1), four solid carbonate cataclasite samples and two recent water samples (WEB-4 and WEB-9) from Boch et al. (2019). Abbreviation for carbonate cataclasite type 1 = type 1 and for carbaonte cataclasite type 2= type 2.

Sample-ID	$\delta^{25}Mg$ [‰ DSM3]	±2σ	$\delta^{26}Mg$ [‰ DSM3]	±2σ	n
IRMM-009	-2.60	0.07	-5.06	0.17	5
CAM1	-1.34	0.09	-2.60	0.11	5
JDO1	-1.09	0.08	-2.04	0.19	3
type 2 (3-C-3)	-1.15	0.13	-2.08	0.26	4
type 2 (3-B-4)	-1.31	0.08	-2.33	0.16	4
type 1 (4-A-9)	-0.99	0.06	-1.77	0.11	4
type 2 (4-A-16)	-0.93	0.06	-1.73	0.15	4
WEB-4	-0.69	0.06	-1.29	0.08	4
WEB-9	-0.54	0.03	-1.01	0.05	4

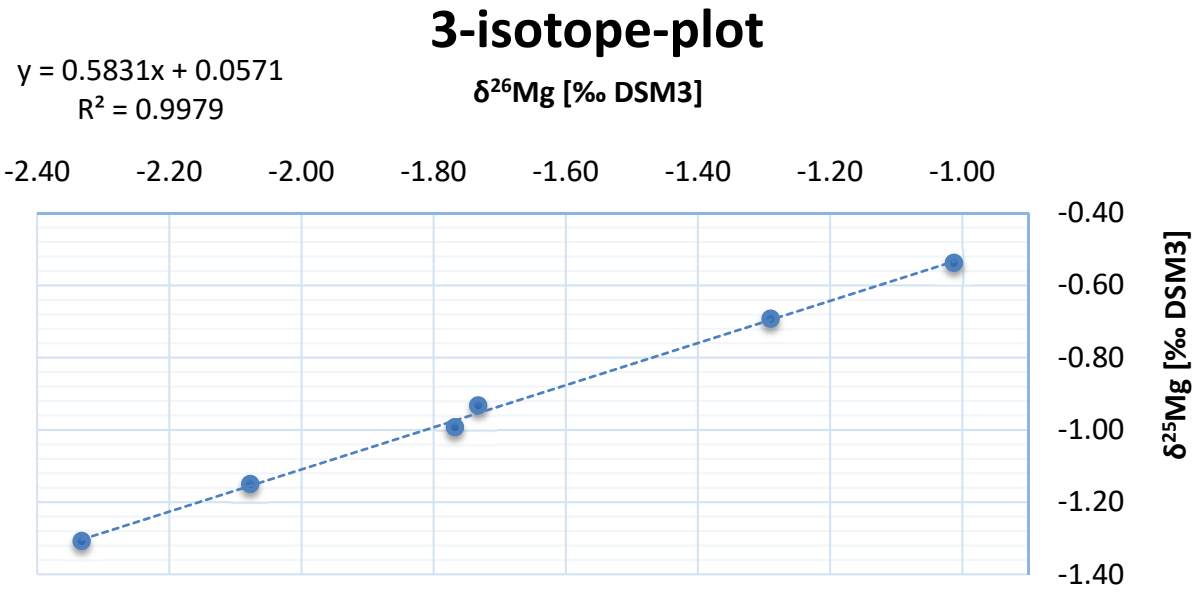

Fig. S 1: 3-isotop-plot for Mg isotopes: $\delta^{25}Mg$ vs. $\delta^{26}Mg$ values should all be on one line due to mass-dependence fractionation. Therefore, the slope must be near 0.5 otherwise problems during the cation separation process or during MS measurement have to be considered.

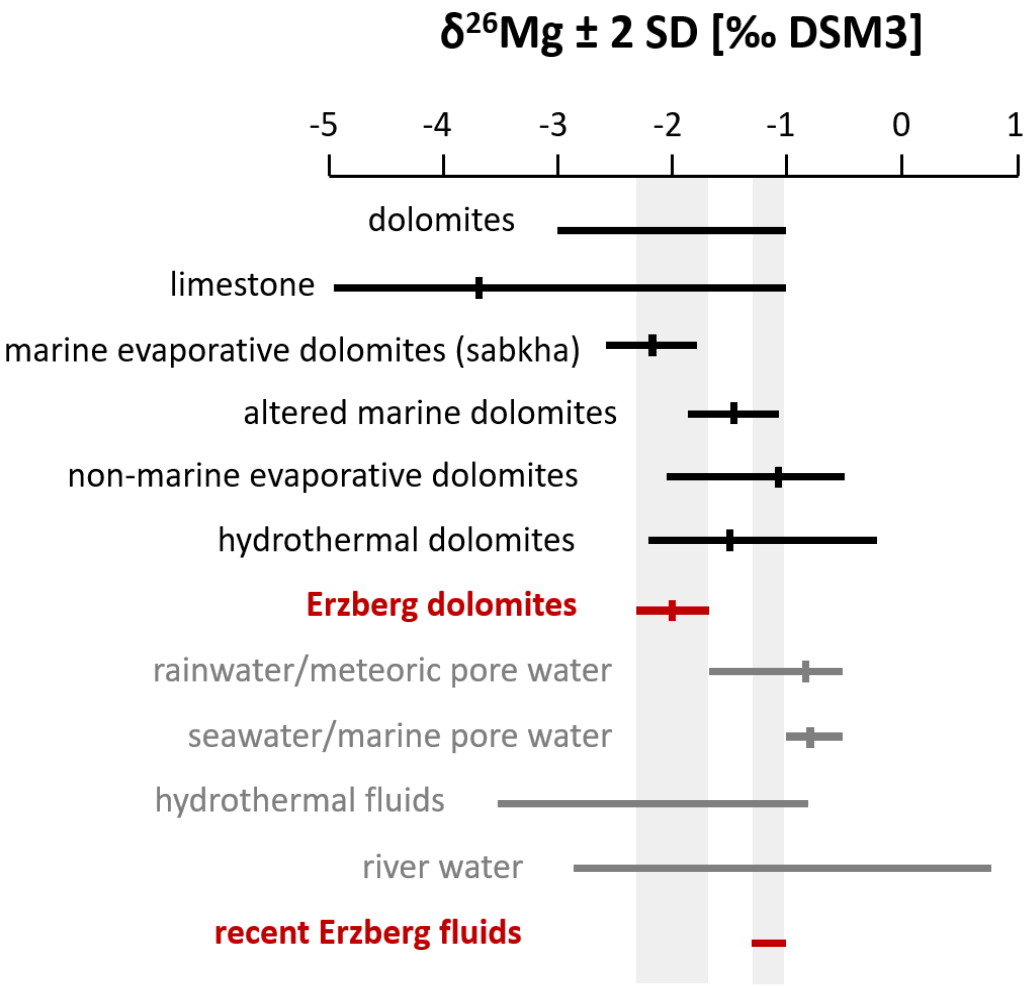

Fig. S 2: Various types of dolomites and their corresponding ranges of $\delta^{26}Mg$ isotope values. The illustration clearly shows that Erzberg dolomite samples plot in an area that fits well from former described fields. The same applies to the analyzed water samples from the Erzberg

Sr-Isotopes

Table S 8: unpublished data from A. Baldermann. $^{87}Sr/^{86}Sr$ ratios for the host rock (Sauberger Kalk), the central & northern fluid (fluid CN), the southern fluid (fluid S), as well as for the dark brown carbonate cataclasite (DB), the light beige carbonate cataclasite (LB), the Erzbergite and the iron ore.

	Min.	Max.	Median	1st quartile	3rd quartile
Host rock	0,70973	0,71127	0,71025	0,70998	0,71068
Fluid CN	0,71528	0,71578	0,71572	0,71571	0,71575
Fluid S	0,71756	0,71756	0,71756	0,71756	0,71756
DB	0,71906	0,72004	0,71942	0,71924	0,71973
LB	0,71724	0,71859	0,71784	0,71754	0,71821
Erzbergite	0,71652	0,71918	0,71798	0,71725	0,71858
Iron ore	0,71933	0,72225	0,71975	0,71954	0,72100

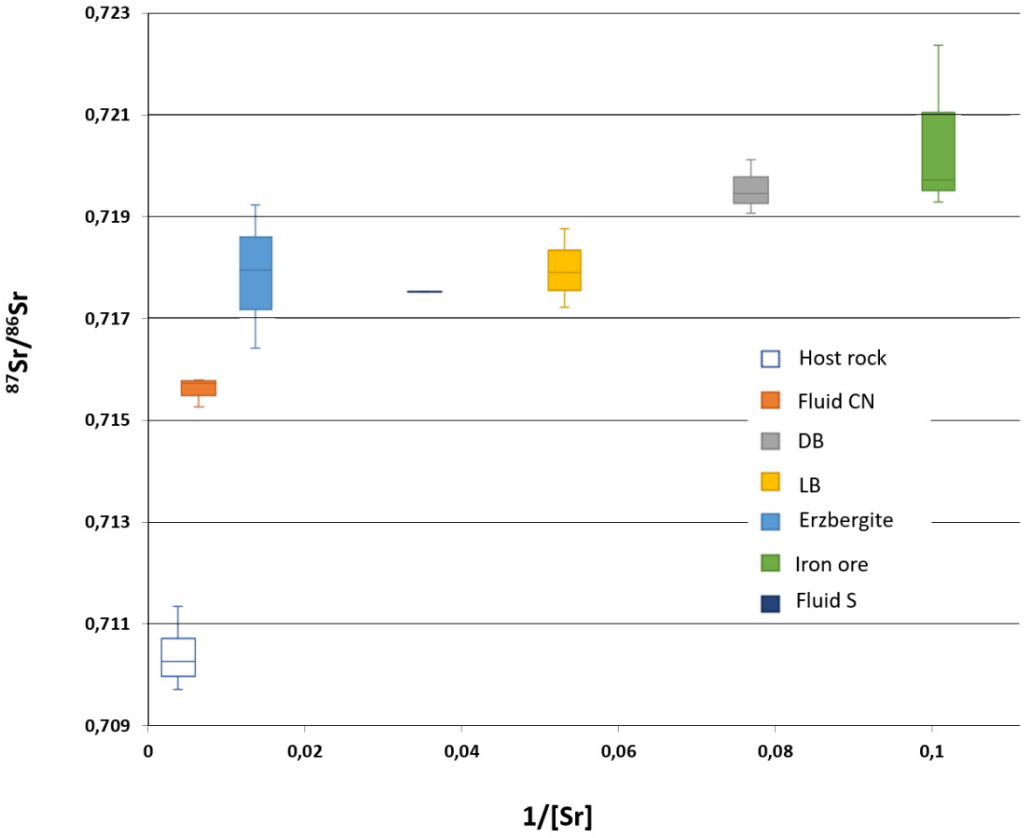

Fig. S 3: Sr-isotope plot showing the position of the two endmembers (i) host rock (Sauberger Kalk) and (ii) iron ore. Modern waters as well as the precipitates erzbergite and the two carbonate cataclasites have formed by dissolution of both endmembers but exhibit different mixtures and concentrations of the two endmembers in this system.

EMPA BSE images, element mappings and quantitative measurements

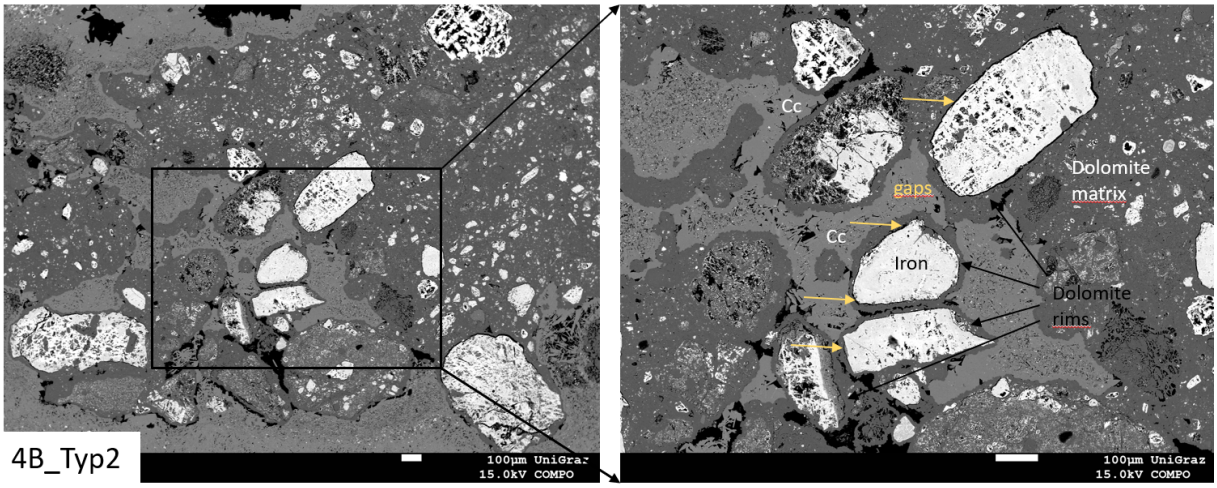

Fig. S 5: BSE image with detail few. Different carbonates are distinguishable by variable grey nuances. Dolomite appear in dark grey whereas calcite and aragonite consist of a bright grey. Yellow arrows mark special gaps between the iron-rich white grains and matrix dolomite seems to growth around them. Within this complex matrix with secondary carbonate fillings, there is still visible porosity (in black).

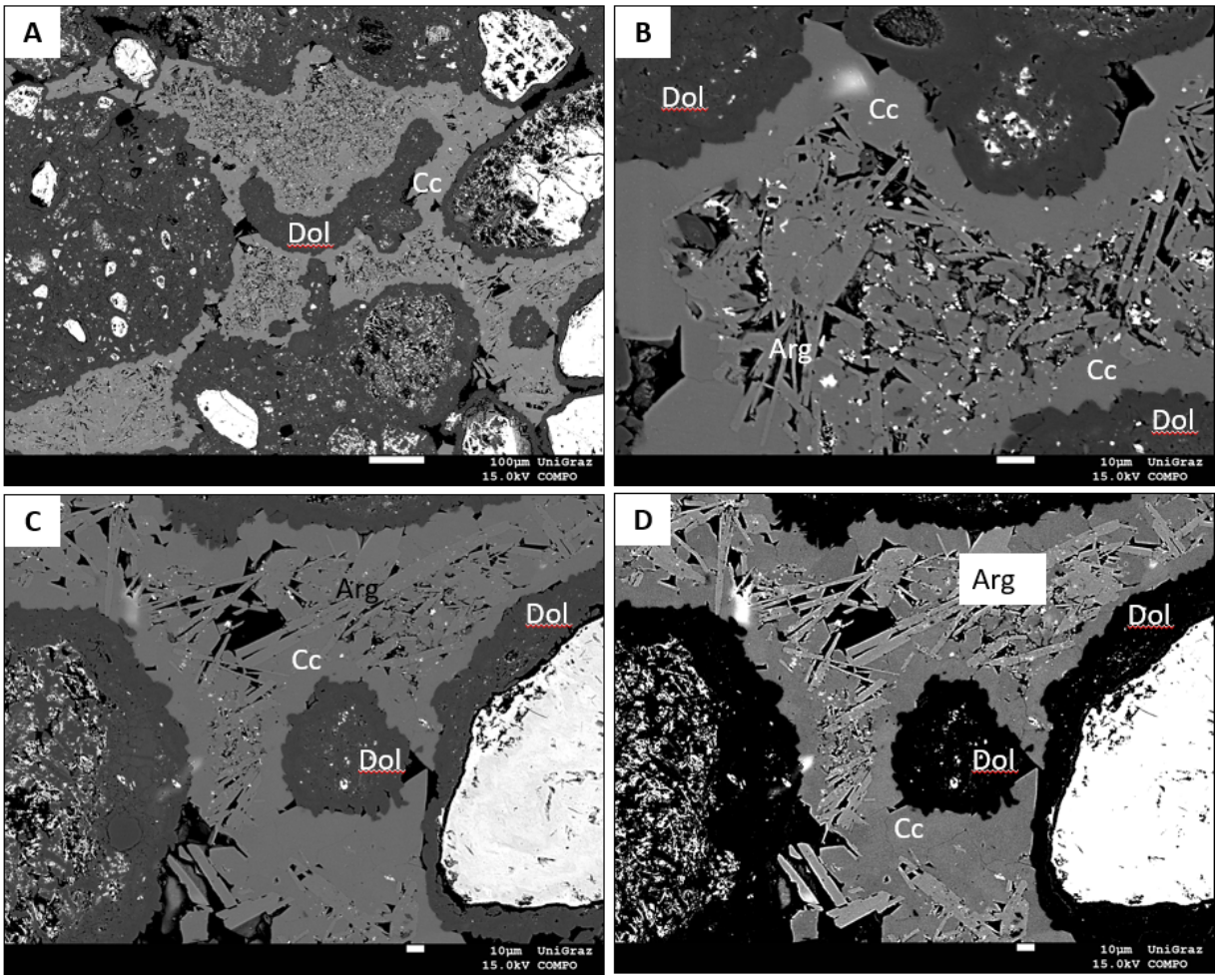

Fig. S 4: : BSE images of sample 4B. A: Detail showing various secondary carbonate precipitates. B-D: With stronger contrast settings dolomite (Dol), calcite (Cc) and aragonite (Arg) can be distinguished by the varying grey colors.

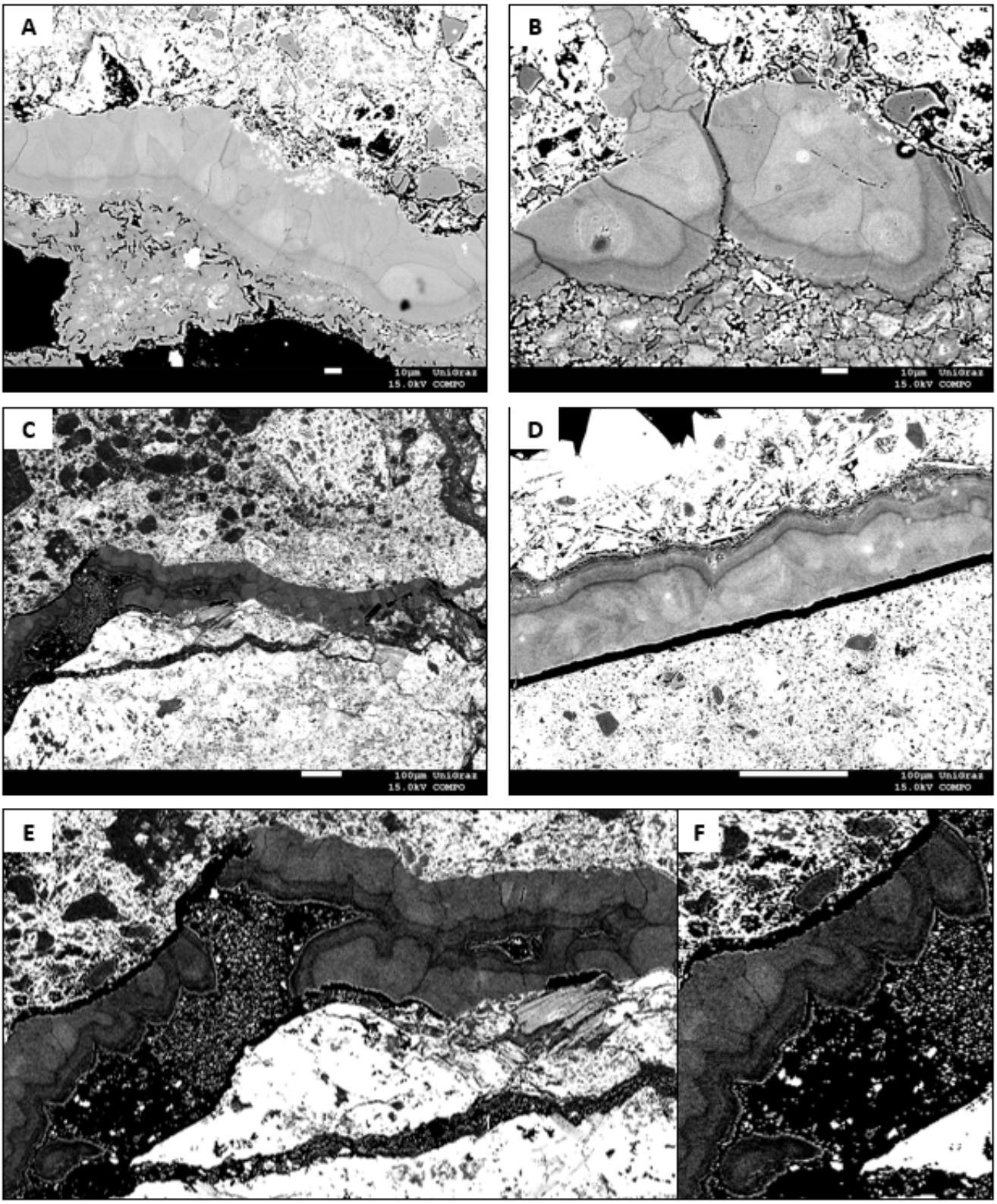

Fig. S 6: BSE images that shows zonation within the spheroidal dolomite grains in the sample EB9.

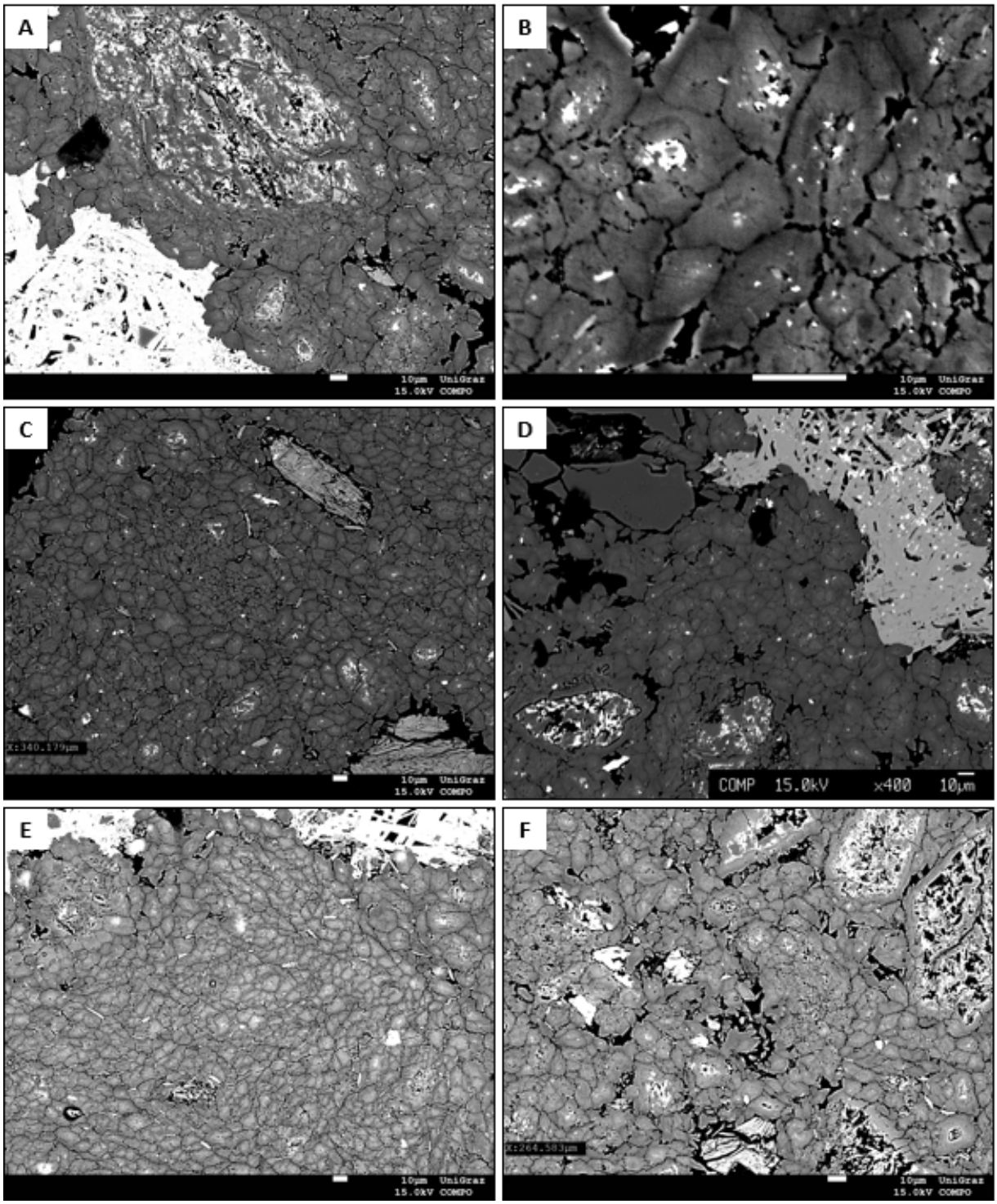

Fig. S 7: Various images of matrix dolomite in the carbonate cataclasite type 1. Aragonite needles are still preserved in the dolomite matrix.

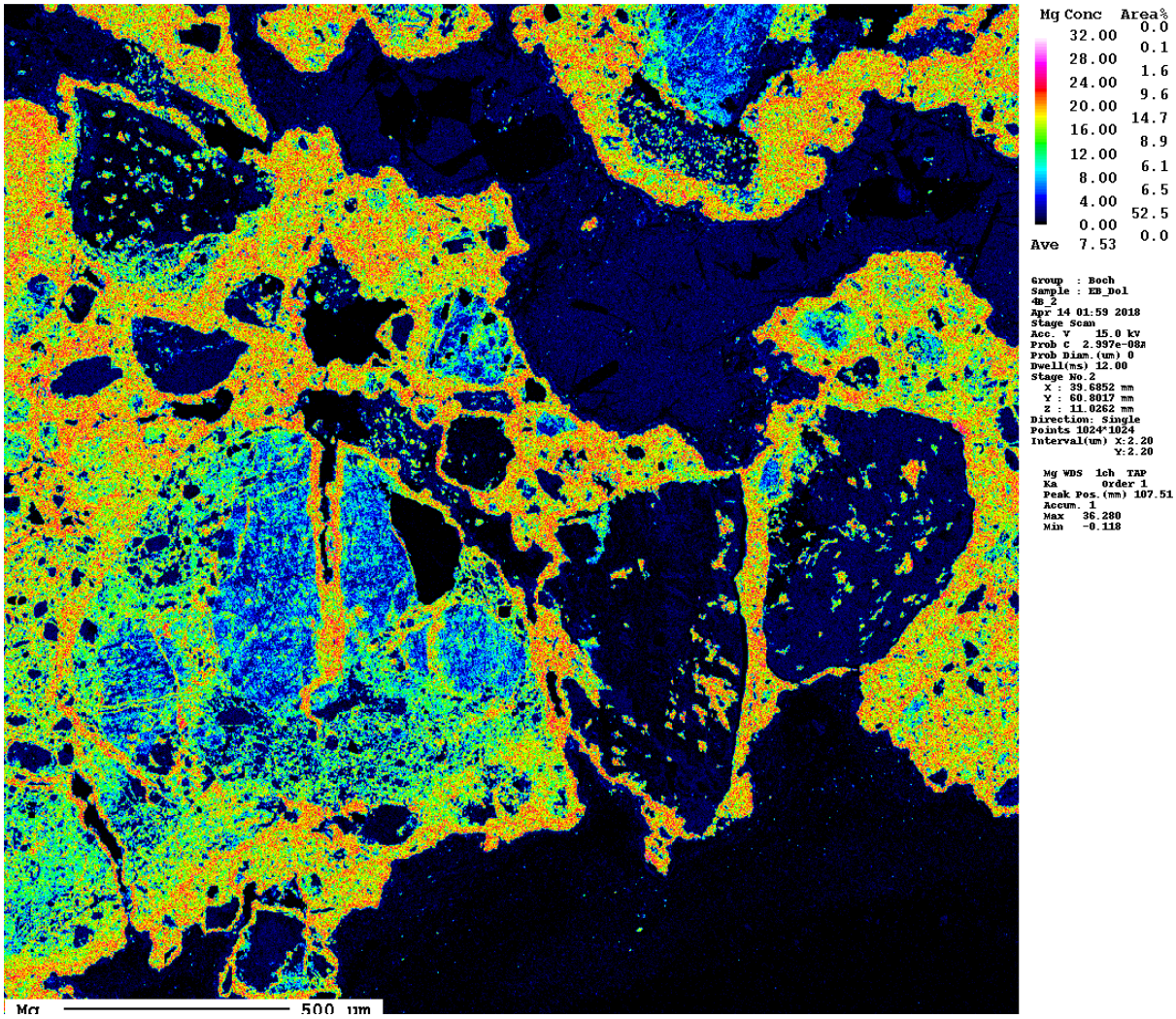

Fig. S 8: Element mapping of Mg from the dark brown carbonat cataclastite layer. Mg distribution clearly shows areas with higher Mg content (e.g. in and around clasts).

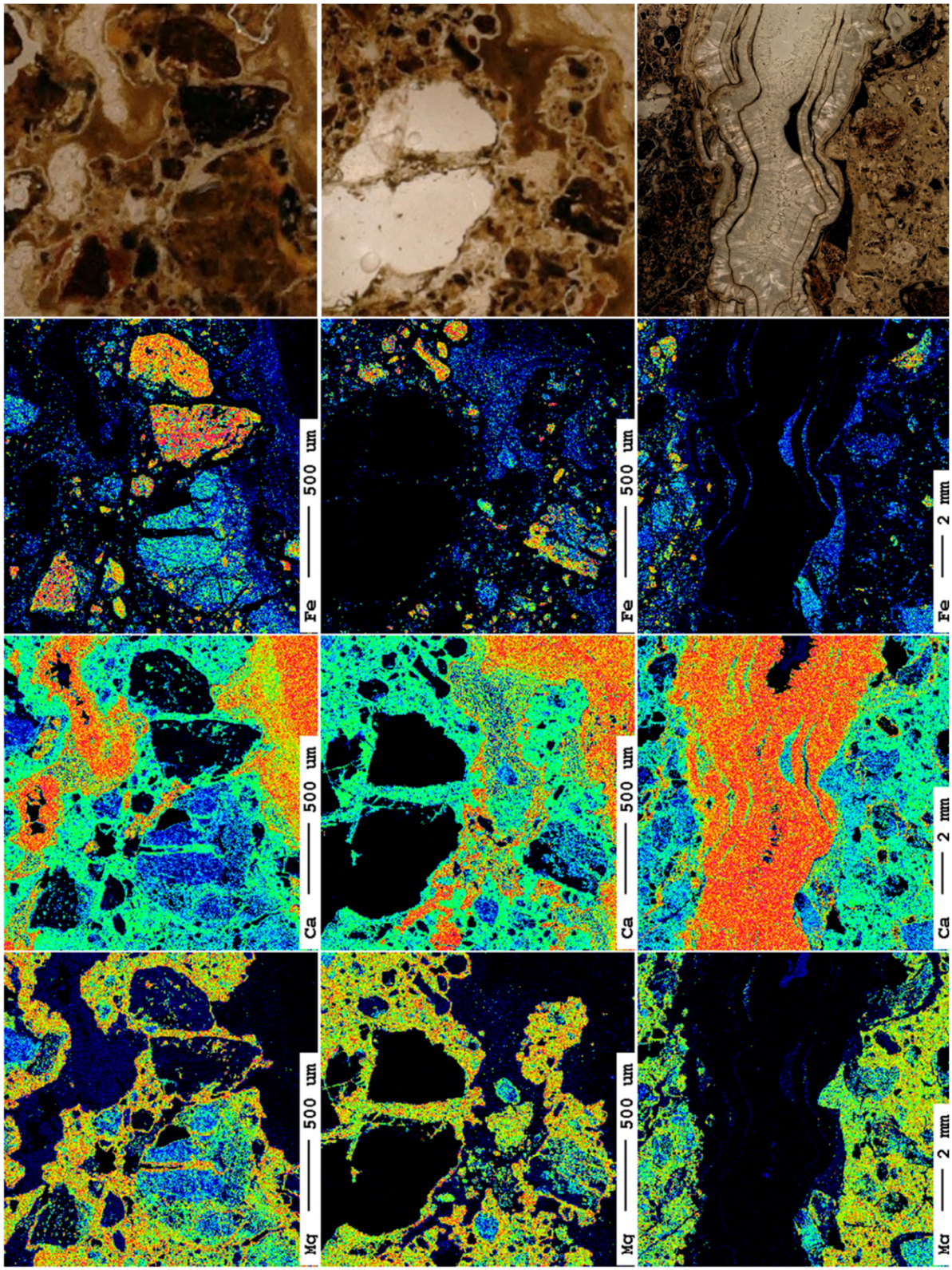

Fig. S 9: Element mappings of three different areas within the sample 4B showing the element distribution maps of Fe, Ca and Mg with their corresponding light microscope detail. Fe-rich grains are identified by high Fe concentrations. Obvious calcite and aragonite (erzbergite) appear in areas where the Ca concentrations yield its maximum (orange colour). Even laminations and growth directions of erzbergite are possible to see (right pictures). High Mg concentrations mainly occur in fissures and around grains (left and middle sequence of images).

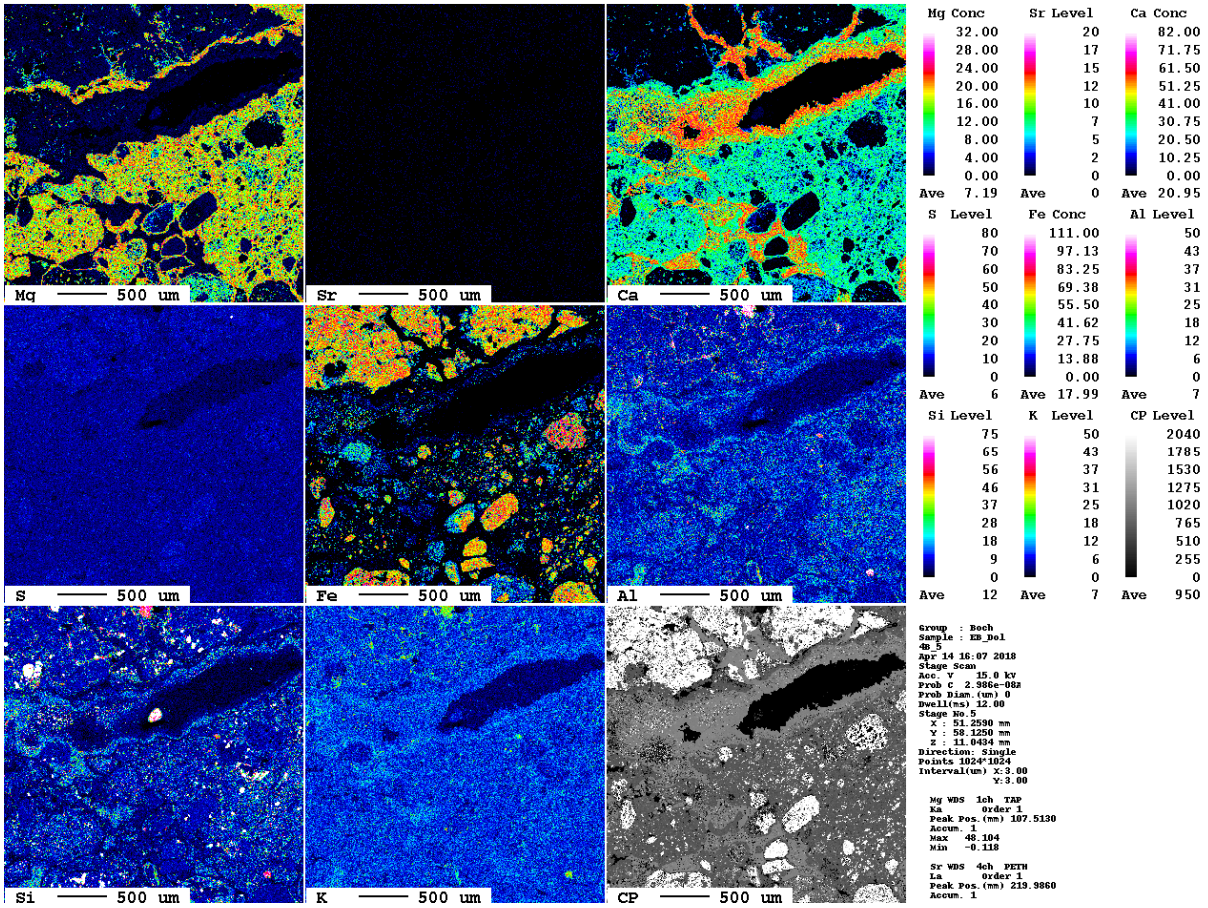

Fig. S 10: Element distribution maps of sample 4B (dark brown carbonate cataclasite).

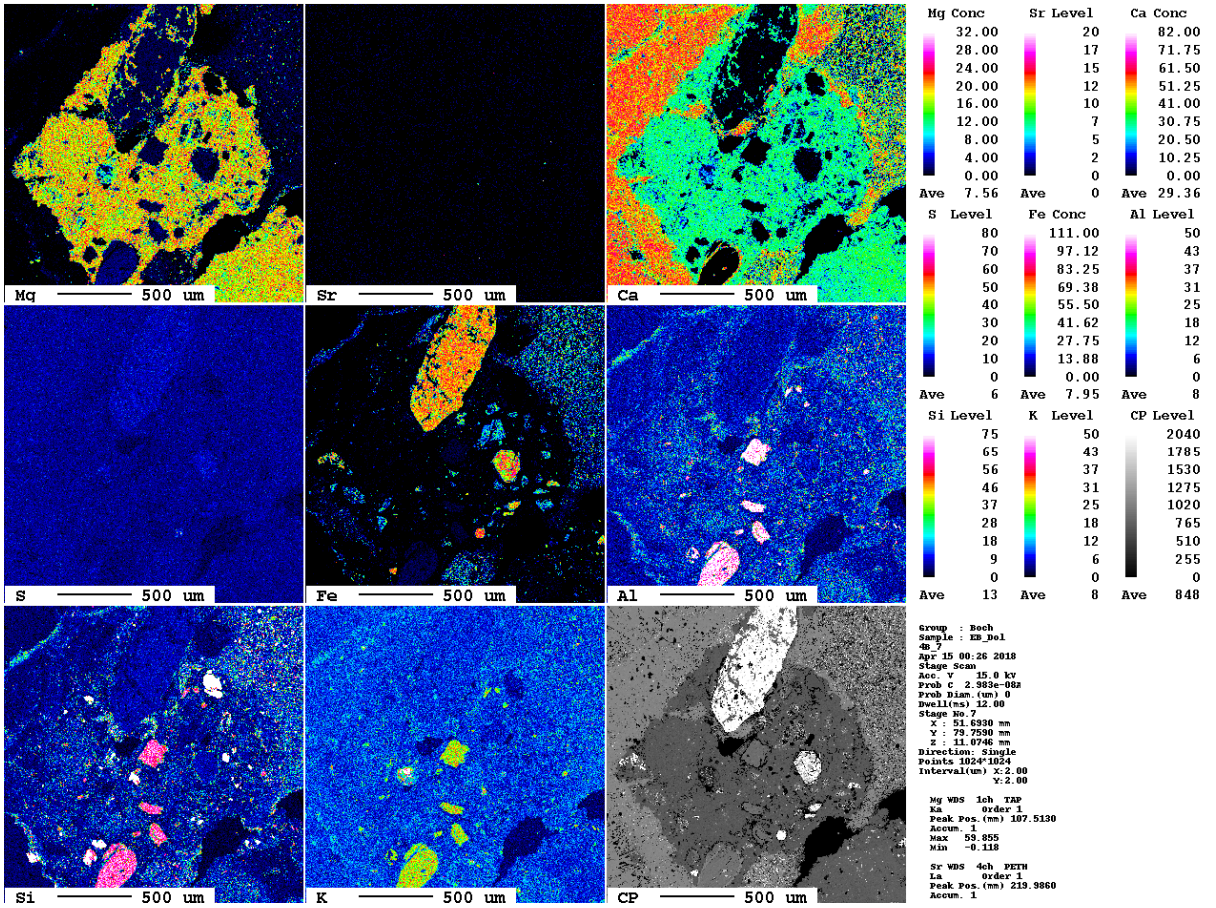

Fig. S 11: Element distribution maps of sample 4B (light beige carbonate cataclasite).

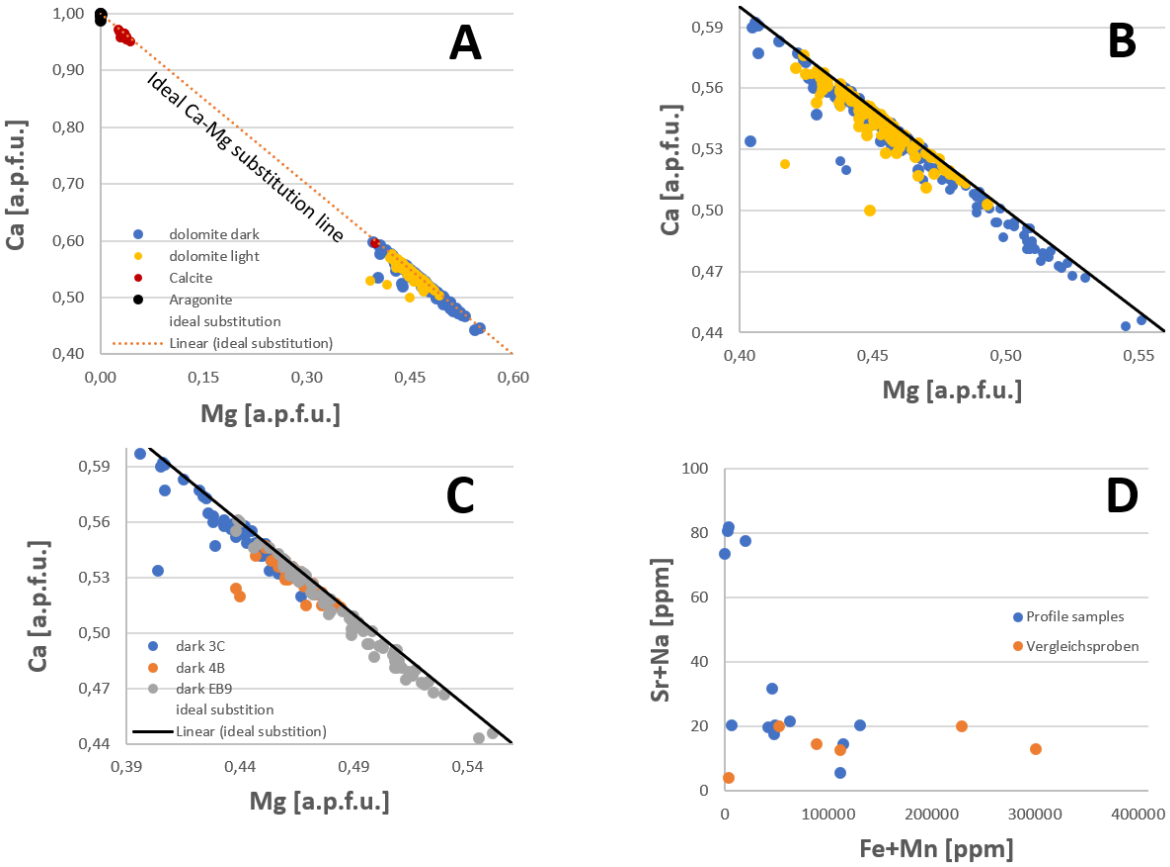

Fig. S 12: Correlation between major and trace elements in the carbonate cataclastic samples, analyzed by EMPA (n=309). A: Cross-plot of Ca and Mg in a.p.f.u., including the ideal Ca-Mg substitution line for carbonates (dotted line). B: Detail view of A. The two types of the dolomite overlap in a wide range and plot near the ideal Ca-Mg- substitution line but are shifted to Ca-excess dolomite. C: Difference between the dark brown dolomite types. D: Correlation between Na+Sr versus Fe+Mn revealed by ICP-OES.

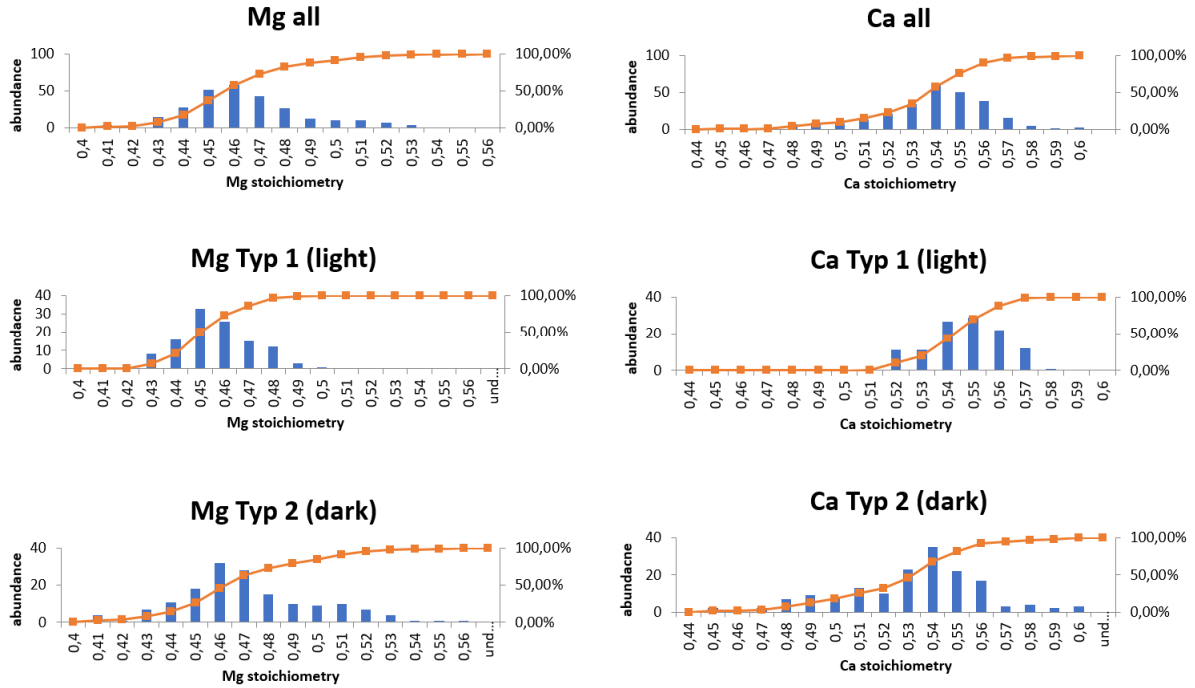

Fig. S 13: Histograms showing the various stoichiometric ratios of Mg and Ca in different dolomite types. The most abundant Mg:Ca ratio is 0.46:0.54.